Journal of Geoscience and Environment Protection, 2025, 13(9), 125-157
https://www.scirp.org/journal/gep
ISSN Online: 2327-4344
ISSN Print: 2327-4336

Climate Change and Surface Water Availability in West Africa: A Case Study of the Diaguiri River Basin

Ibrahima Thiaw

Laboratory of Hydrology and Morphology, Department of Geography, Faculty of Letters and Human Sciences, Cheikh Anta Diop University of Dakar, Dakar, Senegal

Email: ibrahima4.thiaw@ucad.edu.sn

How to cite this paper: Thiaw, I. (2025). Climate Change and Surface Water Availability in West Africa: A Case Study of the Diaguiri River Basin. *Journal of Geoscience and Environment Protection, 13,* 125-157.
https://doi.org/10.4236/gep.2025.139007

Received: July 31, 2025
Accepted: September 22, 2025
Published: September 25, 2025

Abstract

This study evaluates the projected impacts of climate change on surface water availability in the Diaguiri River Basin, a sub-catchment of the Gambia River in West Africa, using the conceptual rainfall-runoff model GR4J. The model was calibrated (1981-1992) and validated (1998-2004) with daily hydroclimatic observations, and forced with bias-corrected outputs from five CORDEX-Africa CMIP5 Regional Climate Models (GFDL-ESM2M, HadGEM2-ES, IPSL-CM5A-LR, MIROC5, and NorESM1-M) under RCP4.5 and RCP8.5 scenarios. Model performance was satisfactory across multiple metrics (NSE = 0.66 - 0.71; KGE = 0.71 - 0.83; logNSE = 0.54 - 0.77). Future simulations reveal a non-linear precipitation-runoff response, with ensemble mean annual discharge increasing by +24.3%, +20.0%, and +30.7% under RCP4.5 for the near-term (2021-2040), mid-century (2041-2070), and late-century (2071-2100), respectively, driven by moderate increases in precipitation anomalies (+6.72%, +5.79%, and +12.16%). Under RCP8.5, streamflow anomalies are more erratic—+45.3%, +35.0%, and +26.5% across the same time slices—despite a declining precipitation signal (+13.68%, +10.19%, and +5.32%), reflecting amplified hydrological sensitivity and non-stationarity. Monthly hydrographs indicate earlier onset of runoff, intensified wet-season flows, and increased intra-annual variability, particularly under RCP8.5, which exhibits elevated skewness and kurtosis, signaling a higher frequency of hydrological extremes. The Diaguiri Basin's strong rainfall-runoff coupling, compounded by scenario- and model-dependent uncertainties, underscores the vulnerability of West African headwater catchments to climate-induced hydroclimatic shifts. The results highlight the urgent need to integrate ensemble-based projections and seasonal regime alterations into adaptive water resource planning and flood risk management frameworks under non-station-

ary climate conditions.

Keywords

CORDEX-Africa, Climate Change, Diaguiri River Basin, Hydrological Modeling, Surface Water Availability

1. Introduction

In the context of accelerating climate change, the management of water resources has become increasingly problematic, particularly in regions that are already prone to significant hydrological variability, such as West Africa (Bodian et al. 2018; Thiaw et al., 2021). The challenges are compounded by the increasing frequency and intensity of climate extremes, which exacerbate the unpredictability of water availability. Recent studies have shown that changing rainfall patterns, rising temperatures, and increasing evapotranspiration are key drivers of this growing uncertainty, putting direct pressure on the hydrological balance and water-dependent systems (Ayugi et al., 2020; Thiaw et al., 2021; Sadio et al., 2023). In sub-humid areas such as southeastern Senegal, these impacts are especially severe due to the strong dependence of rural livelihoods and fragile ecosystems on surface water resources for agriculture, livestock, and domestic use (Faye & Mendy, 2018; Bodian et al., 2018; Thiaw, 2020).

To understand and anticipate the impacts of climate change on river flows and watershed hydrology, hydrological models have become indispensable tools. These models simulate how catchments respond to climatic variables such as precipitation and temperature, which are increasingly being sourced from General Circulation Models (GCMs) and Regional Climate Models (RCMs) operating under various greenhouse gas concentration trajectories (Quesada-Chacón et al., 2021; Kotlarski et al., 2014). While GCMs provide valuable insights at a global scale, their relatively coarse spatial resolution, typically ranging from 100 to 300 kilometers, limits their effectiveness for impact studies at the watershed or local scale (Zubler, Schär, & Lüthi, 2016). RCMs, with spatial resolutions between 10 and 50 kilometers, offer a more detailed representation of regional and local climatic processes. This is particularly important in West Africa, where convective rainfall systems dominate and require finer resolution to be accurately modeled (Teutschbein &Seibert, 2012). Despite these advancements, climate projections still carry considerable uncertainties due to the range of possible emission scenarios, the internal variability of the climate system, and differences in model structures and assumptions. Addressing these uncertainties through multi-model ensembles and statistical bias correction techniques is crucial to improve the robustness of climate impact assessments (Piani et al., 2010; Ayugi et al., 2020). The complexity of West African climate is further amplified by the interplay between large-scale atmospheric circulations and regional features such as the West Afri-

can monsoon. This dynamic system governs the seasonal distribution and intensity of rainfall in the region and poses additional challenges for climate modeling (Sylla et al., 2015; Dosio, 2017). The CORDEX-Africa initiative provides a consistent framework for generating downscaled regional climate projections using a suite of RCMs driven by different GCMs. These RCMs have shown improved performance in reproducing observed climate patterns in Africa, including precipitation gradients and variability (Nikulin et al., 2012; Ehret et al., 2012). When used in conjunction with hydrological models, they enable the simulation of future streamflow conditions under different climate change scenarios.

Hydrological models vary widely in their structure and complexity, and their selection depends on the objectives of the study, data availability, and the scale of application. Broadly, they can be classified into three main categories: empirical, conceptual, and physically based models. Empirical models rely on statistical relationships between inputs and outputs, often derived from observed data, and tend to be simpler but less adaptable to changing conditions (Beven, 2012). Conceptual models, such as GR4J (Perrin et al., 2003), represent the hydrological cycle through simplified reservoirs and parameterized processes, striking a balance between physical understanding and practical applicability, which makes them particularly suitable for data-scarce regions like the crystalline basement zones of West Africa (Bodian et al., 2018; Thiaw, 2020). Physically based models simulate the detailed processes of water movement through soil, vegetation, and river networks using physical equations, requiring extensive input data and computational resources but providing high-resolution insights into hydrological dynamics (Refsgaard & Knudsen, 1996; Beven, 2012). Given the limited availability of hydrological and meteorological data in many parts of West Africa, conceptual models like GR4J are often preferred for regional-scale impact assessments because they effectively capture the essential rainfall-runoff dynamics with relatively few parameters and manageable data requirements (Bodian et al., 2018). Their ability to incorporate bias-corrected climate projections from RCMs enhances the reliability of hydrological simulations, enabling robust assessments of future water availability under climate change.

Simulating river discharge under future climatic conditions, especially in tropical regions characterized by high interannual and seasonal variability (Nka et al., 2015; Thiaw, 2020), demands a robust and scientifically sound modeling framework. Such frameworks must effectively integrate climate projections with hydrological models to generate reliable assessments of future water resources. However, raw outputs from climate models, including both Global Climate Models (GCMs) and Regional Climate Models (RCMs), often exhibit systematic biases due to model limitations, simplifications, and scale mismatches (Maraun et al., 2010; Teutschbein & Seibert, 2012). These biases, if uncorrected, propagate through hydrological simulations and can significantly distort the estimation of river discharge, leading to misleading conclusions about future hydrological regimes. To address these issues, bias correction techniques are applied to climate model outputs before their use in hydrological modeling. Among the various methods, the Cumulative Distribution Function trans-

form (CDF-t) approach (Michelangeli et al., 2009; Vrac et al., 2012) is widely recognized for its effectiveness (Sy, 2019; Thiaw, 2020; Thiaw et al., 2021; Sylla, 2015; Gogien, 2023a, 2023b). CDF-t works by mapping the cumulative distribution function of the modeled climate variable onto the observed distribution, adjusting the simulated values so that their statistical properties align with observations while preserving the temporal coherence and interannual variability of the original data. This ensures that corrected time series remain physically consistent and suitable for hydrological impact studies. Beyond CDF-t, several other bias correction and downscaling methods are commonly used. Quantile Mapping (QM), similar in principle to CDF-t, adjusts the modeled data distribution by matching quantiles between simulated and observed datasets. Variants of QM include parametric and non-parametric approaches (Gudmundsson et al., 2012; Cannon et al., 2015). QM is widely used because of its simplicity and effectiveness, but it may alter temporal sequences if not carefully applied. Empirical Statistical Downscaling methods establish statistical relationships between large-scale climate predictors (from GCMs or RCMs) and local climate variables, often through regression or machine learning techniques (Wilby et al., 2004; Vrac et al., 2012). They can generate high-resolution local climate information but require substantial observational data for calibration. Dynamical Downscaling involves running high-resolution RCMs nested within GCMs to produce regional climate information that resolves local physical processes (Giorgi & Mearns, 1999). While powerful, dynamical downscaling remains computationally expensive and can still require bias correction post-processing. The Delta Change or Change Factor Method is a simpler approach that applies projected changes in climate variables (e.g., temperature or precipitation anomalies) from GCMs/RCMs as additive or multiplicative factors to historical observations (Déqué, 2007). It preserves observed variability but assumes stationarity in climate variability patterns. Recent developments also include Multivariate Bias Correction Methods, which incorporate correction of multiple correlated climate variables simultaneously to maintain physical consistency across variables like temperature, precipitation, and humidity (Cannon, 2018; Vrac & Friederichs, 2015). Integrating bias-corrected climate projections into hydrological models like GR4J enhances the capacity to simulate realistic future river discharge patterns, including the identification of periods of hydrological stress (drought) or surplus (flooding). Such integrated frameworks are essential for water resource management and climate adaptation planning in vulnerable tropical catchments, where hydrological responses to climate variability and change can be highly nonlinear and complex (Teutschbein & Seibert, 2012; Thiaw, 2020; Sadio et al., 2023). Thus, the main objective of this study is to assess the potential impacts of climate change on hydrological regimes in the Diaguiri River Basin, located in the southeastern part of Senegal within the West African crystalline basement region. To achieve this, we apply the GR4J conceptual rainfall-runoff model, calibrated using the SCE-UA optimization algorithm, and forced with climate projections from five regional climate models (RCMs) of the CORDEX-Africa initiative under two Representative Concentration Pathways: RCP4.5 and RCP8.5. This study

aims not only to simulate future average and extreme flows up to the year 2100 but also to explore the associated uncertainties across different climate model outputs. Ultimately, the findings are intended to inform decision-making for sustainable water resource planning and climate adaptation strategies in the basin.

2. Study Area

The Diaguiri River Basin is located between latitudes 12˚25' and 12˚45' North and longitudes 11˚40' and 12˚10' West, entirely within the Kédougou region in southeastern Senegal (**Figure 1**). This area belongs to the West African crystalline basement, characterized by low-permeability geological formations that are nonetheless fractured, allowing moderate recharge of aquifers through rainfall infiltration. The basin experiences a tropical climate, transitioning between the southern Sudanian and northern Guinean climatic zones. It is strongly influenced by two major atmospheric circulation centers: the Saint Helena anticyclone, which dominates during the rainy season, and the Egyptian-Libyan anticyclone, coupled with the Saharan thermal depression, prevailing during the dry season. These systems control the seasonal migration of the Intertropical Convergence Zone (ITCZ), which governs the timing and intensity of precipitation. The wet season, extending from May to October, is marked by humid monsoonal winds originating from the Atlantic Ocean under the influence of the Saint Helena anticyclone, creating favorable conditions for rainfall across the basin. Conversely, the dry season, from November to April, is dominated by the Harmattan winds—dry and dusty air masses from the northeast driven by the Egyptian-Libyan anticyclone. These atmospheric dynamics result in a well-defined bimodal climate, with a distinct alternation between wet and dry periods. The average annual temperature is approximately 29˚C, based on records from the Kédougou synoptic station, the only meteorological station in the basin that monitors temperature. Mean annual rainfall is estimated at 1200 mm for the period 1970-2020, with significant interannual variability linked to fluctuations in the West African monsoon system.

3. Materials and Methods

3.1. Observed Data

To assess the impact of climate change on surface water availability in the Diaguiri River Basin, we compiled a comprehensive dataset of observed hydroclimatic variables, including daily rainfall, temperature, and river discharge records from multiple stations distributed across the basin (**Table 1**). The main hydrometric station is located at the Diaguiri road bridge (Lat: 12.63˚N, Long: −12.08˚W), where daily river discharge was recorded from June 15, 1974 to December 31, 2005, with a mean observed flow of 6.30 m^3/s. Rainfall observations were obtained from six meteorological stations within and around the basin, covering various time periods from 1950 to 2016, with mean annual rainfall ranging from 1050 mm at Nepen Diakha to 1233 mm at Kédougou. Temperature data were available from the Kédougou station for the period 1972-2012, with a mean annual temperature of 29˚C. Potential evap-

otranspiration (PET) was estimated using the method proposed by Oudin (2005), resulting in an average PET of 1903 mm/year across the basin. The spatially representative average rainfall across the Diaguiri Basin was derived using Kriging interpolation techniques implemented in the Hydraccess software (Vauchel, 2004). The use of a single temperature station to estimate Potential Evapotranspiration (PET) in the Diaguiri River Basin relies on the assumption that temperature variations at this station adequately represent those across the entire basin. However, this does not account for localized microclimates or spatial temperature variability, which could introduce uncertainty in PET estimation.

Table 1. Inventory of daily observed rainfall and temperature data

ID Station	Lat.	Long.	Alt. (m)	Data Type	Start of Record (dd/mm/yyyy)	End of Record (dd/mm/yyyy)	Mean Observed
Diaguiri at the road bridge	12.63	−12.08	110	Hydrometric	15/06/1974	31/12/2005	6.30 m^3/s
Kédougou	12.13	−12.34	117	Rainfall	01/01/1950	31/12/2016	1233 mm
				Temperature	01/01/1972	31/12/2012	29°C
Saraya	12.78	−11.78	192	Rainfall	01/01/1950	31/12/2013	1174 mm
Laminia	12.62	−12.12	125		01/01/1973	01/01/2015	1151 mm
Nepen Diakha	12.57	−12.07	162		01/01/1989	31/12/2003	1050 mm
Fongolimbi	12.42	−12.02	410		01/01/1963	31/12/2013	1144 mm
Nafadji	12.62	−11.62	185		01/01/1982	31/12/2016	1100 mm

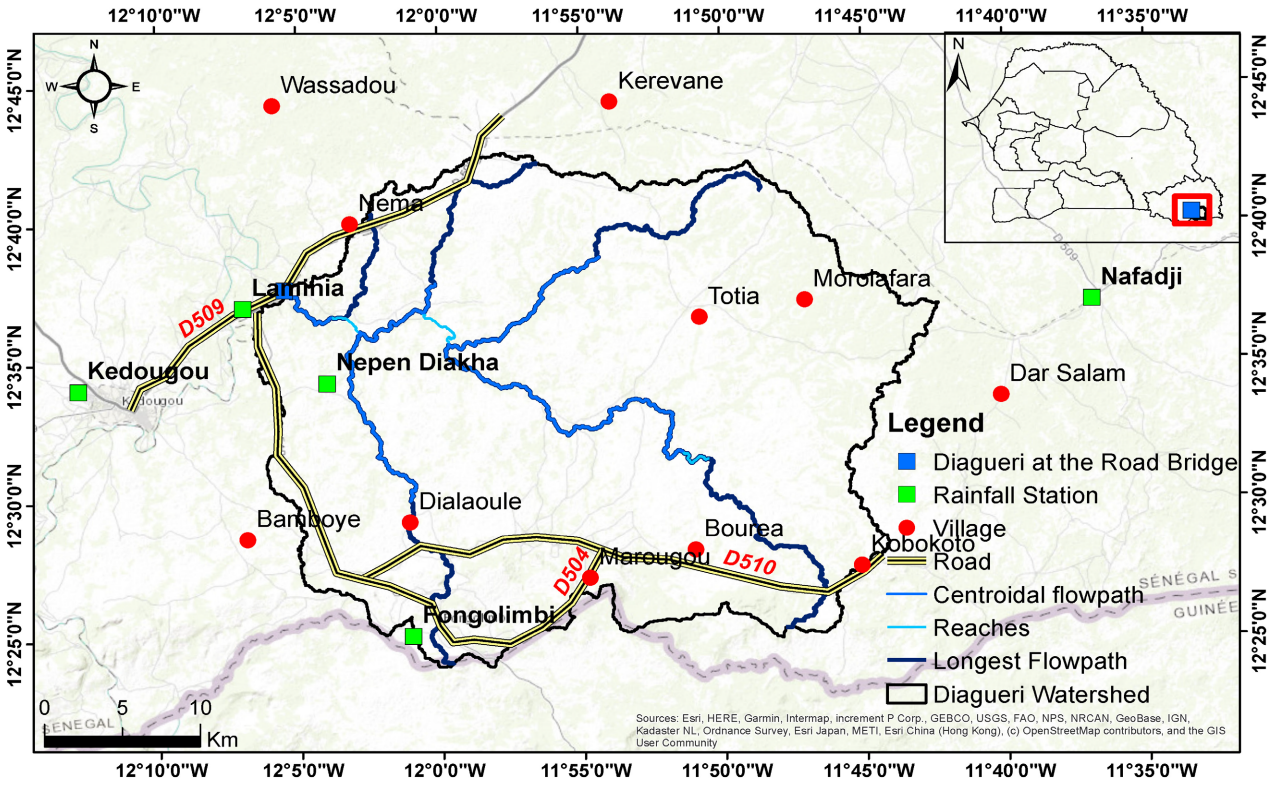

Figure 1. Geographical location of the Diaguiri River Basin and its measurement stations.

3.2. Structure and Functioning of the GR4J Rainfall-Runoff Model

The GR4J (*Génie Rural à 4 paramètres Journalier*) model is a daily lumped rainfall-runoff model developed by Perrin et al. (2003) at the French research institute CEMAGREF (now INRAE). The model adopts a parsimonious approach, relying on just four parameters to characterize the hydrological behavior of a watershed. Its conceptual simplicity and ability to simulate streamflow effectively in catchments with limited hydro-meteorological data make it especially suitable for application in data-scarce watersheds like the Diaguiri River Basin in West Africa. The model employs a parsimonious structure, characterized by only four parameters that capture the essential hydrological behavior of a watershed. These parameters include the production store capacity (X1), which defines the maximum water volume that the soil reservoir can hold; the groundwater exchange coefficient (X2), which accounts for water exchanges with deeper groundwater or adjacent basins; the routing store capacity (X3), which controls the retention of flow within the routing reservoir; and the unit hydrograph time base (X4), which governs the timing and shape of the hydrograph (**Figure 2**). Operating at a daily timestep, the model requires daily inputs of precipitation (*P*) and potential evapotranspiration (*PET*). Rather than spatially discretizing the catchment, GR4J treats it as a lumped, homogeneous unit. Key hydrological processes—including evapotranspiration, infiltration, percolation, and runoff routing—are conceptualized through storage components and transfer functions. The model's architecture features a soil moisture production store that simulates the partitioning of precipitation into net evapotranspiration capacity (*En*) and effective rainfall (*Pn*). This effective rainfall is subsequently split into two flow components: one routed through a unit hydrograph producing rapid runoff (*UH1*), and the other through a secondary hydrograph responsible for delayed flow (*UH2*). These flow components are combined and routed through a routing store (*RS*), which simulates groundwater discharge and attenuates flow peaks (**Figure 2**).

3.3. Cross-Validation Phase of the Model

The calibration and validation of the GR4J hydrological model were carried out using observed daily rainfall (*P*), Potential Evapotranspiration (*PET*), and streamflow data (*Q*) collected from the Diaguiri River Basin. The calibration phase was conducted over the period 1981-1992, while the model validation was performed for the period 1998-2004. To minimize the influence of initial conditions on model outputs, warm-up periods were introduced in 1980 for the calibration phase and 1997 for the validation phase. The exclusion of discharge data from 1993 to 1997 is justified by gaps in the time series or data quality issues that could have skewed the results. By excluding these years, only complete and reliable data are used for calibration and validation, thereby strengthening the robustness of the cross-validation approach and the reliability of future hydrological projections. The model optimization was performed using the Shuffled Complex Evolution-University of Arizona (SCE-UA) algorithm (Duan et al., 1992), which is

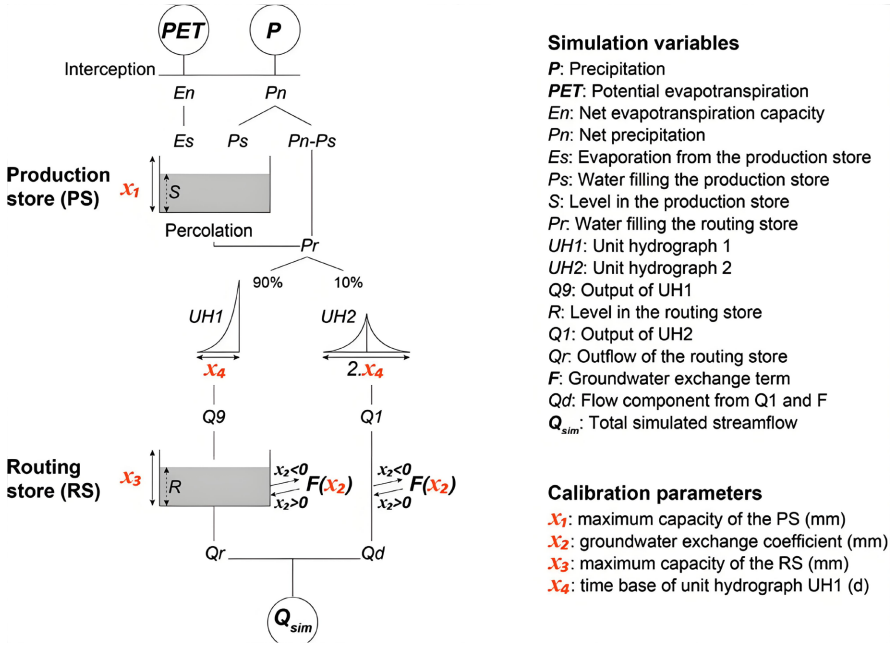

Figure 2. Conceptual scheme of the GR4J model (Perrin et al., 2003).

widely recognized for its robustness in exploring complex parameter spaces and avoiding local optima in hydrological model calibration (Vrugt et al., 2003; Thiaw, 2020; Thiaw et al., 2021). The GR4J model, with its parsimonious structure, requires the careful estimation of its four parameters to adequately capture the hydrological response of the Diaguiri watershed under both historical and future climatic conditions (Perrin et al., 2003; Pushpalatha et al., 2012; Thiaw, 2020). The use of observed data and a rigorous optimization technique ensures the reliability of the calibrated model for subsequent climate change impact assessments on surface water availability in this West African basin.

3.4. Model Performance Evaluation

In this study, the evaluation of the GR4J model's performance in the Diaguiri River Basin was conducted using a multi-objective function that integrates four complementary performance metrics: Nash-Sutcliffe Efficiency (NSE), log-transformed Nash-Sutcliffe Efficiency (log-NSE), Kling-Gupta Efficiency (KGE), and the coefficient of determination (R^2). The combined use of these metrics allows for a more comprehensive and balanced assessment of the model's ability to reproduce both high-flow and low-flow conditions under varying hydrological regimes (Nash & Sutcliffe, 1970; Gupta et al., 2009; Pushpalatha et al., 2012; Kling et al., 2012). The inclusion of both NSE and log-NSE is especially important to capture the model's sensitivity to extreme flows as well as baseflows, particularly in a watershed characterized by strong seasonality and alternating periods of floods and droughts. NSE evaluates the overall agreement between observed and simulated streamflows, with values approaching 1 indicating better model performance (Nash & Sutcliffe, 1970; Moriasi et al., 2007). The log-NSE, by applying a

logarithmic transformation to both observed and simulated flows, enhances the evaluation of low-flow conditions that are critical for water availability during dry seasons (Pushpalatha et al., 2012). The KGE metric, proposed by Gupta et al. (2009), integrates correlation (r), bias (β), and variability (α), providing a global diagnostic of model behavior across different flow regimes. Finally, R^2 measures the strength of linear correlation between observed and simulated discharges, offering a simple indicator of the model's overall fit (Legates & McCabe, 1999). The corresponding mathematical formulations of these performance metrics are as follows:

$$NSE = 1 - \frac{\left[\Sigma\left(Q_{obs,i} - Q_{sim,i}\right)^2\right]}{\left[\Sigma\left(Q_{obs,i} - \bar{Q}_{obs}\right)^2\right]} \tag{1}$$

$$R^2 = \frac{\left[\Sigma\left(\left(Q_{obs,i} - \bar{Q}_{obs}\right)\left(Q_{sim,i} - \bar{Q}_{sim}\right)\right)\right]^2}{\left[\Sigma\left(Q_{obs,i} - \bar{Q}_{obs}\right)^2 * \Sigma\left(Q_{sim,i} - \bar{Q}_{sim}\right)^2\right]} \tag{2}$$

$$\log - NSE = 1 - \frac{\left[\Sigma\left(\log\left(Q_{obs,i}\right) - \log\left(Q_{sim,i}\right)\right)^2\right]}{\left[\Sigma\left(\log\left(Q_{obs,i}\right) - \log\left(\bar{Q}_{obs}\right)\right)^2\right]} \tag{3}$$

$$KGE = 1 - \sqrt{\left[(r-1)^2 + (\alpha-1)^2 + (\beta-1)^2\right]} \tag{4}$$

where $Q_{obs,i}$ and $Q_{sim,i}$ are the observed and simulated streamflows at time step i, respectively; $\bar{Q}_{obs}$ and $\bar{Q}_{sim}$ are their corresponding mean values; r is the linear correlation coefficient; α is the variability ratio (i.e., the ratio of standard deviations $\sigma_{sim}/\sigma_{obs}$); and β is the bias ratio μ_{sim}/μ_{obs}.

The adoption of multiple performance indicators allows the model evaluation to capture the full range of hydrological variability observed in the Diaguiri watershed. Moreover, the integration of the GR4J model with the SCE-UA optimization algorithm (Duan et al., 1992) within airGR (Coron et al., 2017) provides a robust and adaptable framework, particularly well-suited for simulating climate-change scenarios using bias-corrected outputs from Regional Climate Models (RCMs).

3.5. Downscaling of Regional Climate Models

Future climate scenarios were developed using bias-corrected outputs from a suite of Regional Climate Models (RCMs) produced under the CORDEX-Africa initiative (Coordinated Regional Downscaling Experiment for Africa), which provides dynamically downscaled simulations at approximately 0.44˚ resolution suitable for basin-scale climate impact assessments in Africa (Giorgi et al., 2009; Nikulin et al., 2012). These RCMs, driven by different Global Climate Models (GCMs) under the RCP4.5 and RCP8.5 scenarios, were selected for their demonstrated skill in representing the seasonal and interannual variability of the West African monsoon (Nikulin et al., 2012; Sylla et al., 2013; Dosio et al., 2015; Diallo et al., 2016;

Thiaw et al., 2021). The table below summarizes the climate models used in this study.

Table 2. Description of Regional Climate Models (RCMs) and Their Driving GCMs Used

Model	Institution	Model Type	Resolution	Key Features	Simulation Periods	Reference
GFDL-ESM2M	Geophysical Fluid Dynamics Laboratory (USA)	Earth System Model	1.25˚ × 1.25˚	Includes interactive carbon cycles in the ocean and atmosphere	Historical (1950-2005); Future (2021-2100)	Dunne et al., 2012
HadGEM2-ES	Hadley Centre (UK Met Office)	Earth System Model	1.875˚ × 1.25˚	Simulates atmospheric dynamics, ocean currents, and biogeochemical feedback.	Historical (1950-2005); Future (2021-2100)	Collins et al., 2011
IPSL-CM5A-LR	Institut Pierre-Simon Laplace (France)	Earth System Model	2.5˚ × 1.25˚	Integrates atmosphere-ocean-land surface processes	Historical (1950-2005); Future (2021-2100)	Dufresne et al., 2013
NorESM1-M	Norwegian Climate Centre (Norway)	Earth System Model	1.9˚ × 2.5˚	Emphasizes high-latitude feedbacks and carbon cycles.	Historical (1950-2005); Future (2021-2100)	Bentsen et al., 2013
MIROC5	University of Tokyo (Japan)	Earth System Model	1.4˚ × 1.4˚	Coupled model addressing global variability and long-term projections	Historical (1950-2005); Future (2021-2100)	Watanabe et al., 2010

To enhance the physical realism of the climate projections, the raw RCM outputs were bias-corrected using the CDF-t method (Cumulative Distribution Function transform), which adjusts both the mean and higher-order moments of the modeled distribution to match those of observed data while preserving climate change signals (Michelangeli et al., 2009; Vrac et al., 2012). This correction technique has been widely validated and is particularly suited for applications in hydrological impact modeling under climate change conditions (Teutschbein & Seibert, 2012; Thiaw, 2020; Thiaw et al., 2021). The bias correction utilized observed daily data of precipitation (1950-2016) and temperature (1972-2012) from the Diaguiri basin for the historical reference periods. Each climate variable was corrected independently, and the procedure was applied at the scale of each grid cell intersecting the catchment. To aggregate the bias-corrected RCM precipitation grids to basin-scale inputs, the Kriging method was employed using Hydraccess software (Vauchel, 2004). The resulting bias-adjusted time series were then used as inputs to simulate streamflow responses over the future period 2021-2100, which was subdivided into three-time horizons: near-term (2021-2040), mid-century (2041-2070), and end-of-century (2071-2100).

4. Results

4.1. GR4J Model Efficiency during Cross-Validation

The evaluation of the GR4J model's performance during the cross-validation phase highlights its robustness in simulating streamflow within the semi-humid Diaguiri

River Basin. The calibration, conducted over the period 1981-1992, and the subsequent validation, carried out for 1998-2004, enabled an assessment of the model's transferability across distinct climatic conditions. During calibration, the Nash-Sutcliffe Efficiency (NSE) reached 0.66 and improved to 0.71 during validation, indicating good agreement between observed and simulated flows, particularly during the rainy season when runoff generation is most pronounced (Figure 3 and Figure 4). The log-transformed NSE (log-NSE), which emphasizes low-flow dynamics, increased markedly from 0.54 to 0.77, suggesting that the model effectively reproduces both high-flow events and baseflows (Figure 3 and Figure 4)—an essential aspect in semi-humid basins where streamflow is governed by the alternation between wet and dry seasons (Thiaw, 2020; Thiaw et al., 2021). The Kling-Gupta Efficiency (KGE), which integrates correlation, bias, and variability, also showed improvement from 0.71 to 0.83, confirming the model's balanced performance across hydrological components. Similarly, the coefficient of determination (R^2) followed the same trend as the NSE (0.66 and 0.71), further attesting to the reliability of the simulations (Figure 3 and Figure 4).

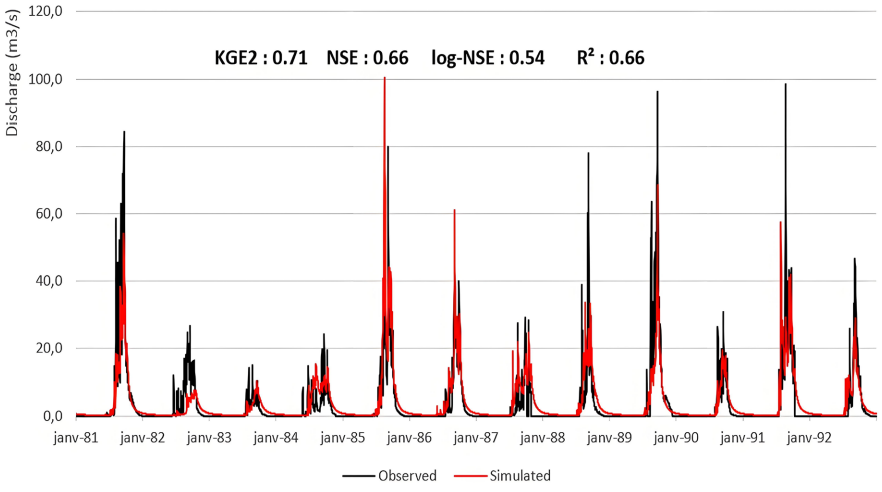

Figure 3. Calibration of the GR4J model over the period 1981-1992.

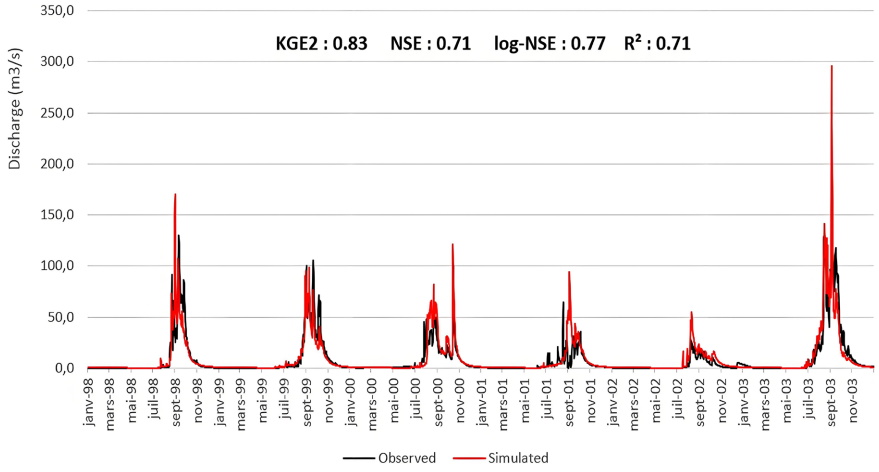

Figure 4. Validation of the GR4J model over the period 1998-2004.

These findings confirm the GR4J model's reliability and suitability for projecting future streamflow under climate change scenarios, thereby reinforcing confidence in the anticipated hydrological shifts within the Diaguiri River Basin. In light of the model's stable and consistent performance, particularly during the validation phase (1998-2004), the corresponding parameter set—X1: 207.40 mm, X2: −30.66 mm, X3: 333.28 mm, and X4: 2.09 days—was retained for future simulations.

4.2. Bias Correction of Climate Projections Using CDF-t

4.2.1. Temperature Bias Correction under RCP4.5 and RCP8.5

The CDF-t bias correction technique was applied separately to the temperature outputs of each climate model, using observed daily data from 1972 to 2012 as a reference period. This approach allowed for the adjustment of the modeled temperature distributions so that they better reflected the statistical characteristics of observed series, notably their mean values and interannual variability. Under the RCP4.5 emissions scenario, bias correction led to noticeable improvements across most models. For instance, GFDL-ESM2M reproduced the observed standard deviation relatively well (2.09˚C versus 2.23˚C observed), with a correlation of 0.73 and a root mean square deviation (RMSD) of 2.12˚C. HadGEM2-ES and IPSL-CM5A-LR performed even better, with correlation coefficients of 0.89 and 0.91, respectively, and RMSD values below 2˚C. Although MIROC5 slightly exaggerated the variability, it retained a low RMSD of 1.65˚C. NorESM1-M yielded the most consistent results, combining the lowest RMSD (1.38˚C) with a high correlation of 0.92. Under the RCP8.5 scenario, model behavior remained broadly similar. GFDL-ESM2M and HadGEM2-ES showed higher RMSDs (2.29˚C and 2.33˚C), while IPSL-CM5A-LR and MIROC5 maintained strong correlation values (0.89) and RMSDs of 2.35˚C and 1.54˚C, respectively. Once again, NorESM1-M provided the most stable results, with a correlation of 0.91 and an RMSD of 1.68˚C (**Figure 5**).

Overall, the CDF-t method significantly improved the alignment between modeled and observed temperature data. Among the ensemble, NorESM1-M, MIROC5, and IPSL-CM5A-LR emerged as the most reliable performers under both RCP4.5 and RCP8.5 scenarios. These improvements in temperature accuracy reinforce the credibility of hydrological projections for the Diaguiri Basin, thereby contributing to more robust planning for climate adaptation and sustainable water management in this key sub-basin of the Gambia River.

4.2.2. Precipitation Bias Correction under RCP4.5 and RCP8.5

The CDF-t method was also applied to precipitation outputs from multiple climate models, using observed rainfall data from 1950 to 2016 in the Diaguiri River Basin as a reference. This bias correction markedly improved the representation of the statistical properties of precipitation, especially its variability and distribution, which are critical for accurately modeling runoff generation and hydrological extremes in climate-sensitive catchments. Under the RCP4.5

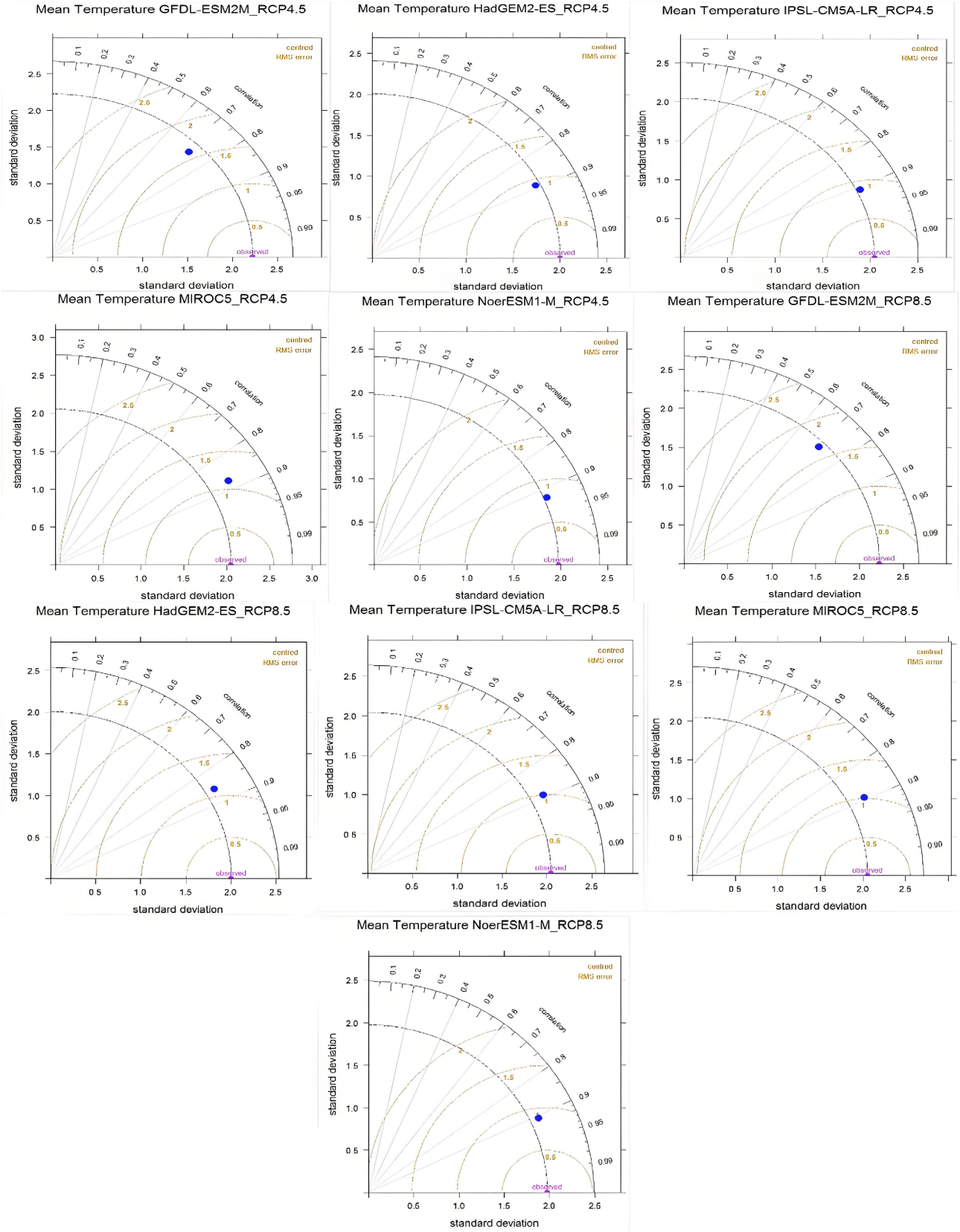

Figure 5. Taylor diagrams comparing CDF-t bias-corrected CMIP5 temperature outputs with observations under RCP4.5 and RCP8.5 scenarios.

scenario, MIROC5 and NorESM1-M showed the best agreement with observed precipitation patterns. Their standard deviations closely matched the observed value of 3.76 mm, with high correlation coefficients of 0.86 and 0.83, respectively, and the lowest root mean square deviations (RMSDs) of 2.22 mm and 2.20 mm. IPSL-CM5A-LR and HadGEM2-ES also performed well, though HadGEM2-ES slightly underestimated interannual variability. GFDL-ESM2M tended to overestimate variability but maintained a reasonable correlation of 0.80, with an RMSD of 2.51 mm. Under the RCP8.5 scenario, overall model performance remained consistent. HadGEM2-ES and NorESM1-M continued to deliver strong results, with RMSDs near 2.15 mm and correlations above 0.83. MIROC5 slightly overestimated variability (4.32 mm) but retained a strong correlation of 0.82. GFDL-ESM2M again had the highest RMSD (2.63 mm), reflecting persistent overestimation, while IPSL-CM5A-LR showed balanced moderate performance (**Figure 6**). These findings highlight the essential role of bias correction in refining climate model outputs for hydrological simulations. Given precipitation's key role as the main driver of hydrological processes in the Diaguiri River Basin, these corrected datasets substantially improve the reliability of simulated runoff, streamflow, and hydrological extremes under future climate scenarios.

4.2.3. Projected Warming Trends over the 21st Century

The projected temperature trends derived from the multi-model ensemble reveal a consistent and progressive warming of the Diaguiri River Basin throughout the 21st century under both RCP4.5 and RCP8.5 scenarios. Under the intermediate stabilization pathway RCP4.5, the mean temperature anomaly relative to the historical baseline increases from +1.29˚C during the near-term period (2021-2040) to +2.01˚C in the mid-century (2041-2070), reaching +2.41˚C by the end of the century (2071-2100) (**Figure 7**). This trajectory reflects a gradual warming trend, aligning with global efforts to limit radiative forcing and greenhouse gas emissions after mid-century. In contrast, under the high-emission RCP8.5 scenario—which assumes continued growth in emissions—the projected warming is more pronounced and accelerates over time. Temperature anomalies begin at +1.45˚C in the near future (2021-2040), rise sharply to +2.66˚C by mid-century (2041-2070), and culminate at a significant +4.37 °C by the late 21st century (2071-2100) (**Figure 8**). This steeper trajectory under RCP8.5 indicates a strong sensitivity of the regional climate system to greenhouse gas forcing, with the latter period exhibiting nearly double the warming compared to RCP4.5.

These results highlight the growing divergence between scenarios after mid-century and underscore the critical influence of future emission pathways on regional climate outcomes. The projected warming—especially under RCP8.5—has profound implications for the hydrological regime of the Diaguiri Basin, including increased evapotranspiration, altered runoff patterns, and heightened stress on water resources.

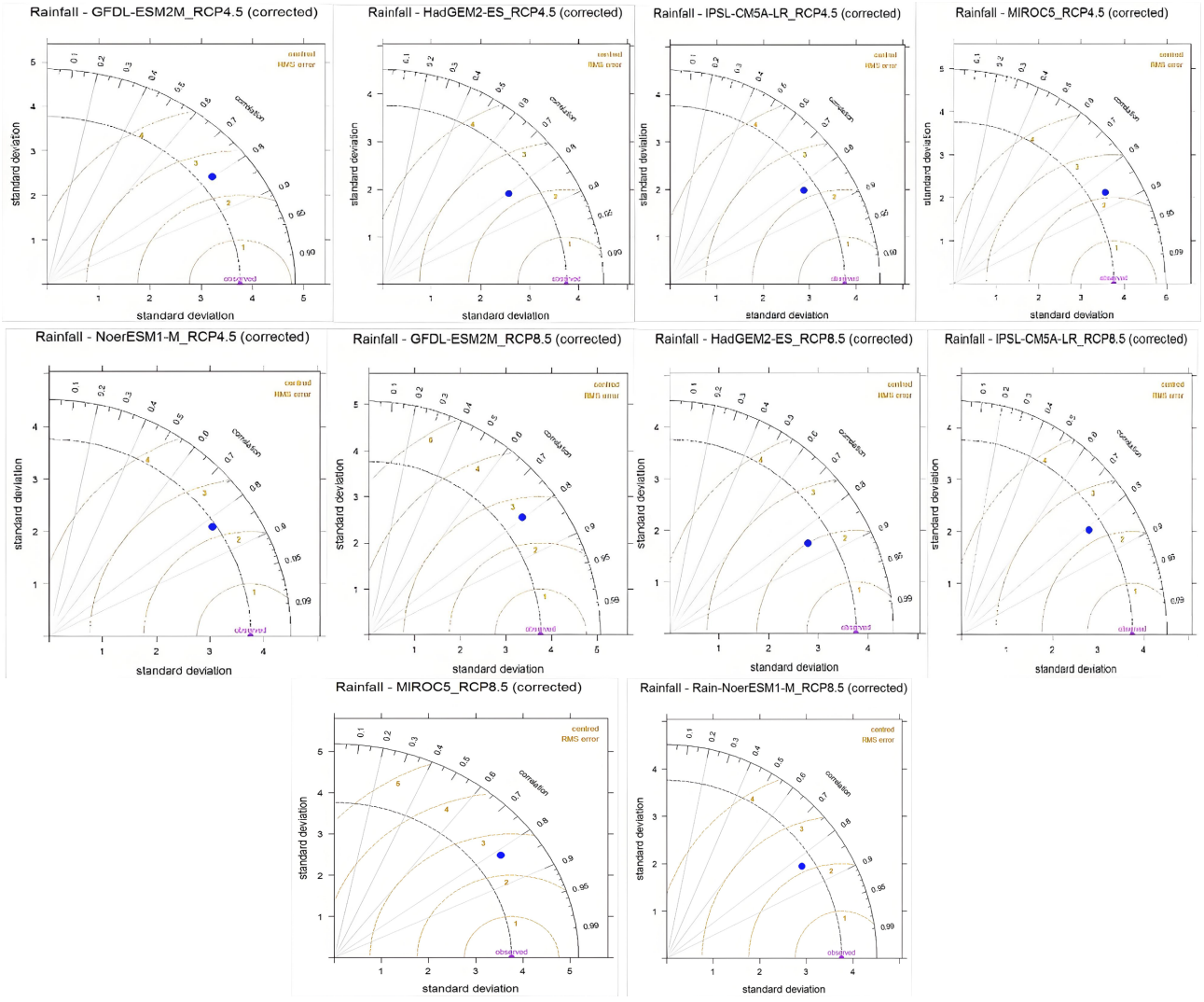

Figure 6. Taylor diagrams comparing CDF-t bias-corrected CMIP5 precipitation outputs with observations under the RCP4.5 and RCP8.5 scenarios.

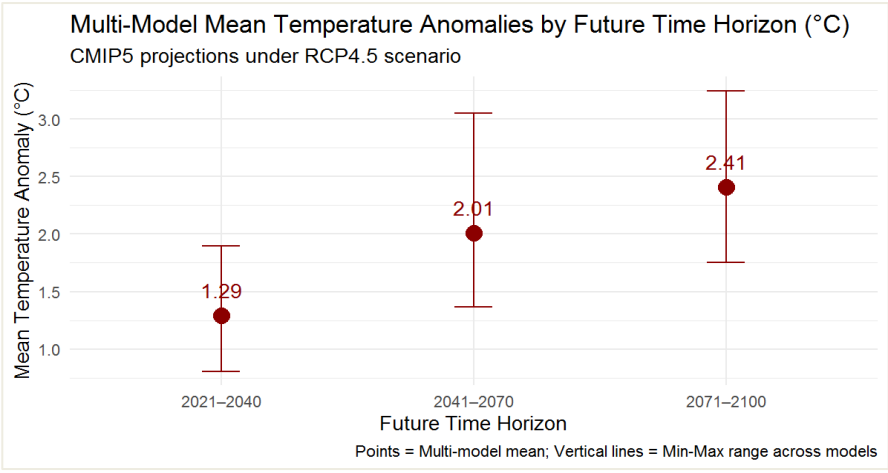

Figure 7. Projected multi-model mean temperature anomalies under RCP4.5 for three future periods: 2021-2040, 2041-2070, and 2071-2100.

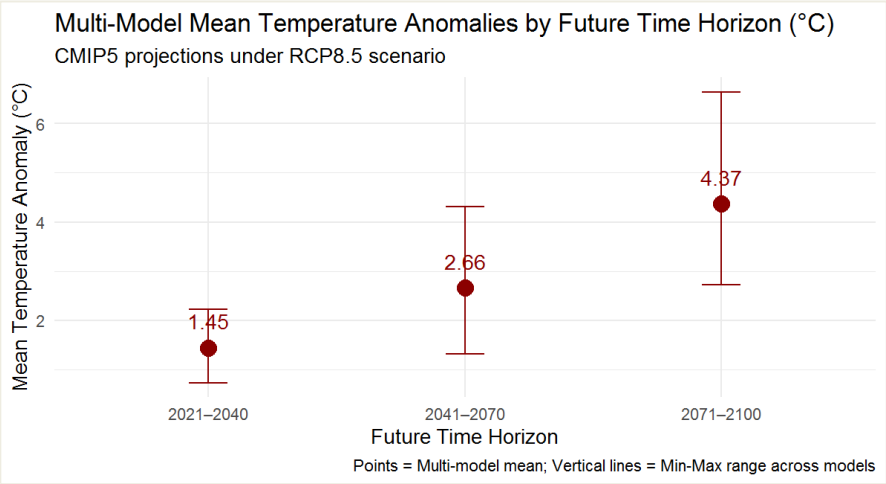

Figure 8. Projected multi-model mean temperature anomalies under RCP8.5 for three future periods: 2021-2040, 2041-2070, and 2071-2100.

4.2.4. Projected Rainfall Evolution through 2100

The projected evolution of precipitation over the Diaguiri River Basin throughout the 21st century, based on bias-corrected outputs from a suite of five CMIP5 global climate models (GFDL-ESM2M, HadGEM2-ES, IPSL-CM5A-LR, MIROC5, and NorESM1-M), reveals marked temporal heterogeneity and pronounced scenario-dependent divergence. Under the RCP4.5 stabilization pathway, ensemble projections indicate a modest but progressively increasing hydroclimatic signal. Mean annual precipitation anomalies relative to the historical baseline (1956-2016) are projected to rise by +6.72% during the near term (2021-2040), with a slight attenuation to +5.79% in the mid-century (2041-2070), followed by a more substantial increase of +12.16% toward the end of the century (2071-2100). This gradual upward trajectory suggests a potential intensification of moisture availability under moderate radiative forcing. However, the inter-model spread remains substantial—ranging from −11.96% (IPSL-CM5A) to +18.48% (HadGEM2-ES) in the near term, and reaching up to +39.89% (MIROC5) by century's end (**Figure 9**). Conversely, the RCP8.5 high-emissions scenario exhibits a more erratic and nonlinear precipitation response, characterized by amplified inter-model variance and weakened convergence. The ensemble mean anomaly peaks early in the century at +13.68% (2021-2040), reflecting a greenhouse gas-driven intensification of the regional hydrological cycle. This signal diminishes to +10.19% by mid-century and further weakens to +5.32% by 2071-2100, despite highly divergent individual model outputs. For instance, while GFDL-ESM2M projects an extreme increase of +62.7% by century's end, HadGEM2-ES and IPSL-CM5A-LR simulate pronounced drying trends of −31.7% and −28.02%, respectively (**Figure 10**). This divergence points to deep model disagreement under strong radiative forcing, likely driven by disparate representations of deep convection, land-atmosphere feedbacks, and large-scale circulation shifts affecting monsoonal dynamics.

Overall, these findings underscore the profound uncertainty inherent in long-

term precipitation projections for the Diaguiri River Basin, particularly under RCP8.5. While RCP4.5 supports a more coherent signal of modest wetting, the high-emissions trajectory entails a shift toward hydroclimatic non-stationarity, with potential for both substantial intensification and severe rainfall deficits depending on the model and time horizon. Given the basin's strong precipitation-runoff coupling, such variability presents critical implications for future hydrological responses, water availability, and flood risk.

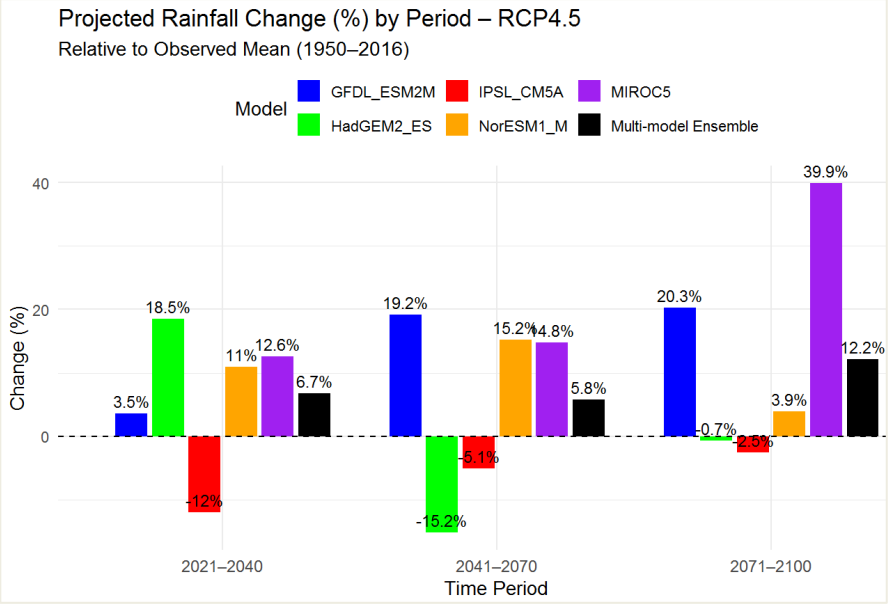

Figure 9. Multi-model ensemble mean and range of projected precipitation anomalies under RCP4.5 for the Diaguiri River Basin (2021-2100).

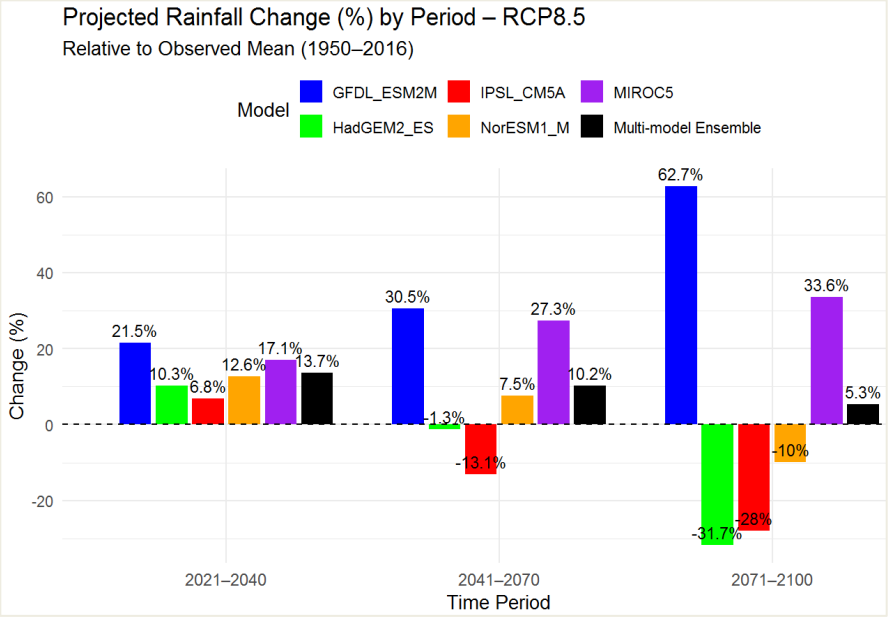

Figure 10. Multi-model ensemble mean and range of projected precipitation anomalies under RCP8.5 for the Diaguiri River Basin (2021-2100).

4.2.5. Projected Changes in Annual Streamflow through to 2100

Under the RCP4.5 stabilization pathway, long-term projections indicate a substantial intensification of annual runoff volumes in the Diaguiri River Basin over the 2021-2100 period. The multi-model ensemble mean (MMM) streamflow is projected to increase by +24% relative to the historical baseline, a response that closely reflects the basin's precipitation-driven hydrological regime (Table 3, Figure 11). This enhanced runoff signal aligns with the ensemble mean precipitation anomaly of +8.37%, based on bias-corrected outputs from five CMIP5 global climate models. However, considerable inter-model variability underscores the system's nonlinear rainfall-runoff response. For instance, MIROC5, which simulates the highest precipitation anomaly (+23.45%, equivalent to +273 mm), yields the most pronounced streamflow amplification (+50.7%), while GFDL-ESM2M follows closely with a +15.6% rainfall increase driving a +45.6% discharge gain. NorESM1-M, with a moderate precipitation rise of +10.0%, produces a corresponding +33% increase in mean annual flow. In contrast, HadGEM2-ES projects a near-stationary precipitation signal (−1.35%) and a marginal discharge increase (+3.9%), while IPSL-CM5A-LR, exhibiting a drying trend (−5.88%), simulates a negative runoff response (−12.9%) (Figure 11). These divergent projections emphasize the Diaguiri Basin's strong hydroclimatic sensitivity and the critical role of antecedent moisture conditions and model-specific rainfall dynamics in modulating future streamflow. The amplification of discharge variability, evident through increases in ensemble spread and higher-order flow statistics, further reflects the basin's potential transition toward hydrological non-stationarity under evolving climate conditions.

Table 3. Baseline and projected annual streamflow variability in the Diaguiri Basin under RCP4.5

Statistic	Observed	GFDL_ESM2M	HadGEM2_ES	IPSL_CM5A_LR	MIROC5	NorESM1_M	MMM_RCP4.5
Mean (m^3/s)	6.16	9.02	6.44	5.40	9.34	8.24	7.69
STD (m^3/s)	3.47	4.87	4.06	3.60	3.79	4.55	4.17
CV	0.56	0.54	0.63	0.67	0.41	0.55	0.56
Skewness	0.63	0.83	1.12	1.04	0.73	0.99	0.94
Kurtosis	−0.15	0.70	1.22	0.63	0.67	1.02	0.85
Min (m^3/s)	0.79	0.72	0.45	0.69	3.01	0.89	1.15
Q05 (m^3/s)	1.80	2.51	1.07	1.10	3.81	2.08	2.11
Q25 (m^3/s)	3.34	5.58	3.74	2.62	6.38	5.69	4.80
Q50 (m^3/s)	5.94	8.28	5.77	4.80	8.82	7.51	7.04
Q75(m^3/s)	8.20	11.87	7.92	7.00	11.49	10.29	9.71
Q95 (m^3/s)	12.07	17.43	14.44	13.29	15.27	17.40	15.56
Max (m^3/s)	15.51	26.34	19.68	16.88	21.93	22.50	21.47
IQR (m^3/s)	4.86	6.29	4.18	4.38	5.11	4.59	4.91
Range (m^3/s)	14.72	25.62	19.22	16.19	18.93	21.62	20.31

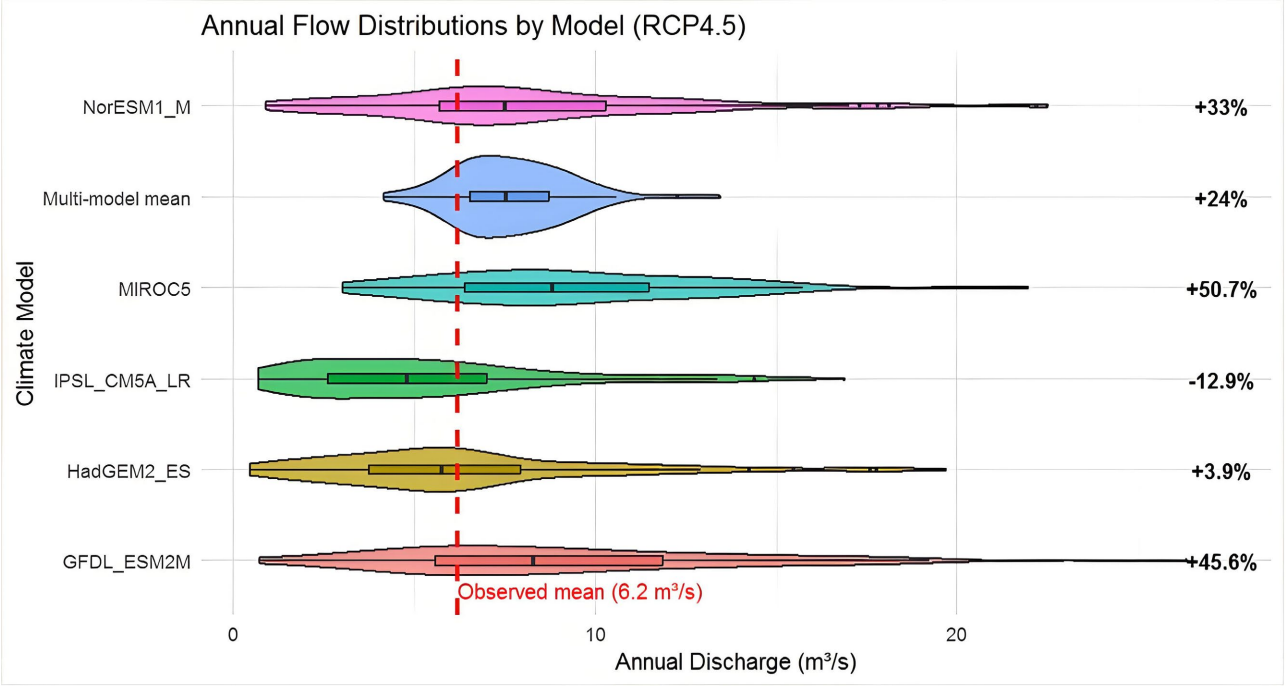

Figure 11. Distribution of Annual Streamflow by Climate Model under RCP4.5 (2021-2100).

While the RCP4.5 scenario outlines a moderately wetter future with relatively consistent precipitation-runoff responses, the RCP8.5 pathway introduces a more complex and heterogeneous hydrological signal, driven by amplified radiative forcing and divergent precipitation trajectories across models. Indeed, by 2100, the multi-model mean (MMM) annual streamflow increases by +34.3%, rising from a historical baseline of 6.20 m^3/s to 8.30 m^3/s. This hydrological amplification corresponds to a +9.3% increase in multi-model ensemble precipitation (from 1164.4 mm to 1272.5 mm), though individual model responses diverge widely. For instance, GFDL-ESM2M, which exhibits the highest projected rainfall anomaly (+40.0%, equivalent to +466 mm), simulates a dramatic +125.7% increase in streamflow, indicating strong nonlinear amplification likely driven by intensified rainfall events and saturation-excess runoff. Similarly, MIROC5, with a +27.0% increase in precipitation, yields a +58.3% discharge rise. In contrast, HadGEM2-ES and IPSL-CM5A-LR simulate notable rainfall deficits (−9.5% and −13.5%, respectively), which translate into reduced streamflows of −4.4% and −21.3% (**Table 4**, **Figure 12**). These disparities underscore the basin's high rainfall-runoff sensitivity and the divergent hydrological pathways that arise from inter-model variability in precipitation projections. Overall, despite a modest ensemble mean increase in rainfall, the streamflow response is amplified in magnitude and variability, pointing to the potential for disproportionate hydrological extremes under future climate conditions—particularly in rainfall-dependent semi-humid systems like the Diaguiri Basin. These findings emphasize the importance of incorporating both ensemble means and model spread into future water resource planning and risk assessment frameworks.

Table 4. Baseline and projected streamflow variability in the Diaguiri basin under RCP8.5.

Statistic	Observed	GFDL_ESM2M	HadGEM2_ES	IPSL_CM5A_LR	MIROC5	NorESM1_M	MMM_RCP8.5
Mean (m^3/s)	6.2	14.0	5.9	4.9	9.8	7.0	8.3
STD (m^3/s)	3.5	7.7	4.4	4.3	3.8	4.2	4.9
CV	0.6	0.6	0.7	0.9	0.4	0.6	0.6
Skewness	0.6	0.9	1.2	0.7	0.6	0.6	0.8
Kurtosis	−0.2	1.3	1.8	−0.7	0.3	0.1	0.6
Min (m^3/s)	0.8	0.2	0.2	0.2	1.7	0.7	0.6
Q05 (m^3/s)	1.8	4.0	0.6	0.3	4.2	1.2	2.1
Q25 (m^3/s)	3.3	8.2	2.8	1.1	7.4	3.4	4.6
Q50 (m^3/s)	5.9	13.3	5.0	3.4	9.0	7.0	7.5
Q75(m^3/s)	8.2	18.5	7.7	7.8	12.2	9.6	11.1
Q95 (m^3/s)	12.1	27.8	13.6	12.7	16.3	13.8	16.8
Max (m^3/s)	15.5	43.0	23.0	16.0	22.0	19.3	24.6
IQR (m^3/s)	4.9	10.3	4.9	6.7	4.8	6.2	6.6
Range (m^3/s)	14.7	42.7	22.8	15.8	20.3	18.6	24.0

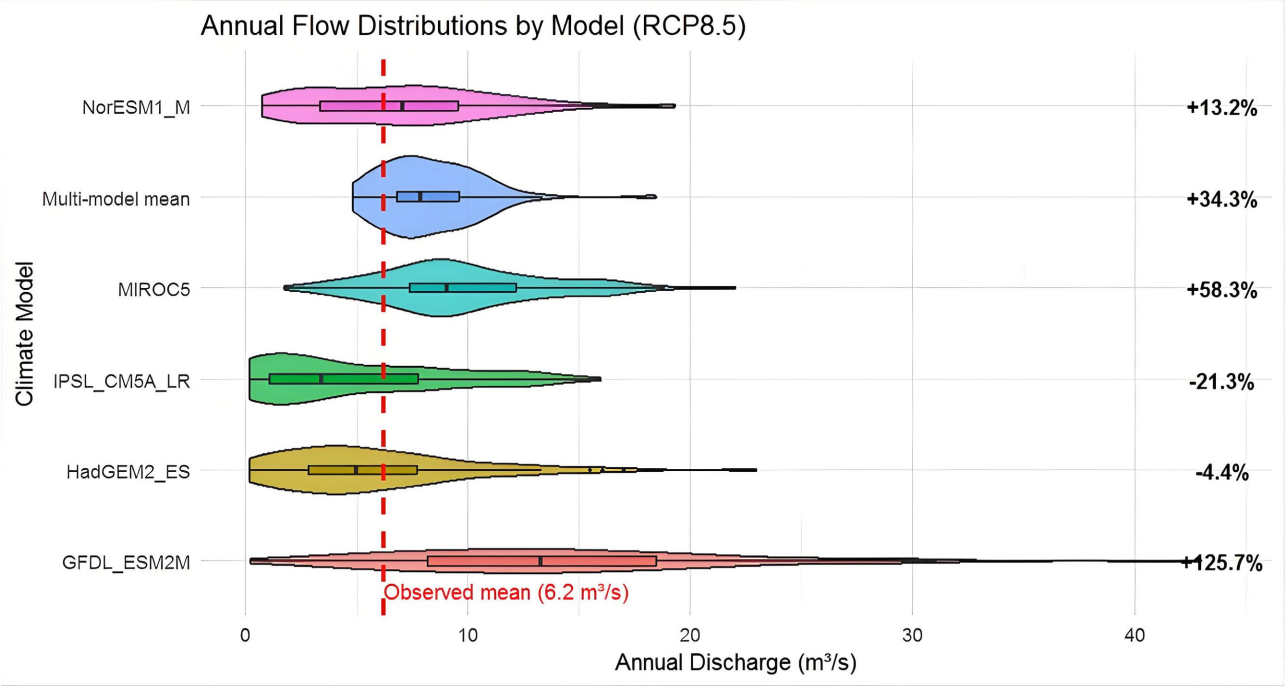

Figure 12. Distribution of Annual Streamflow by Climate Model under RCP8.5 (2021-2100).

4.2.6. Century Streamflow Dynamics by Sub-Period

The multi-model mean streamflow projections for the Diaguiri River Basin under the RCP4.5 and RCP8.5 scenarios highlight distinct temporal variability across three key sub-periods of the 21st century. Under the RCP4.5 scenario, the multi-model mean (MMM) streamflow increases by +24.3% in the near term (2021-2040), stabi-

lizes at +20% by mid-century (2041-2070), and intensifies further to +30.7% in the late-century period (2071-2100). These hydrological shifts are consistent with the progressive increase in ensemble mean precipitation anomalies—rising from +6.72% to +12.16%—and reflect a coherent intensification of moisture availability under moderate radiative forcing. In contrast, under RCP8.5, the hydrological response exhibits a more erratic trajectory, shaped by highly divergent rainfall projections. While streamflows initially surge to +45.3% in the near term, they decline to +35% mid-century and further to +26.5% by century's end, mirroring the weakening precipitation signal (+13.68% to +5.32%). This declining hydrological signal occurs despite some models projecting extreme increases in rainfall (e.g., GFDL-ESM2M: +62.7%), while others simulate severe drying (e.g., HadGEM2-ES: −31.7%). The broader inter-model spread in rainfall anomalies under RCP8.5 translates into greater hydrological uncertainty, with streamflow distributions exhibiting increased dispersion, asymmetry, and peakedness. Overall, the Diaguiri Basin's strong rainfall-runoff coupling underscores the critical importance of accounting for precipitation variability in projecting future hydrological behavior. The contrasting patterns observed between scenarios point toward a wetter, yet more predictable future under RCP4.5, versus a more volatile and uncertain regime under RCP8.5—raising essential challenges for water resources planning and flood risk mitigation in the context of climate-driven non-stationarity.

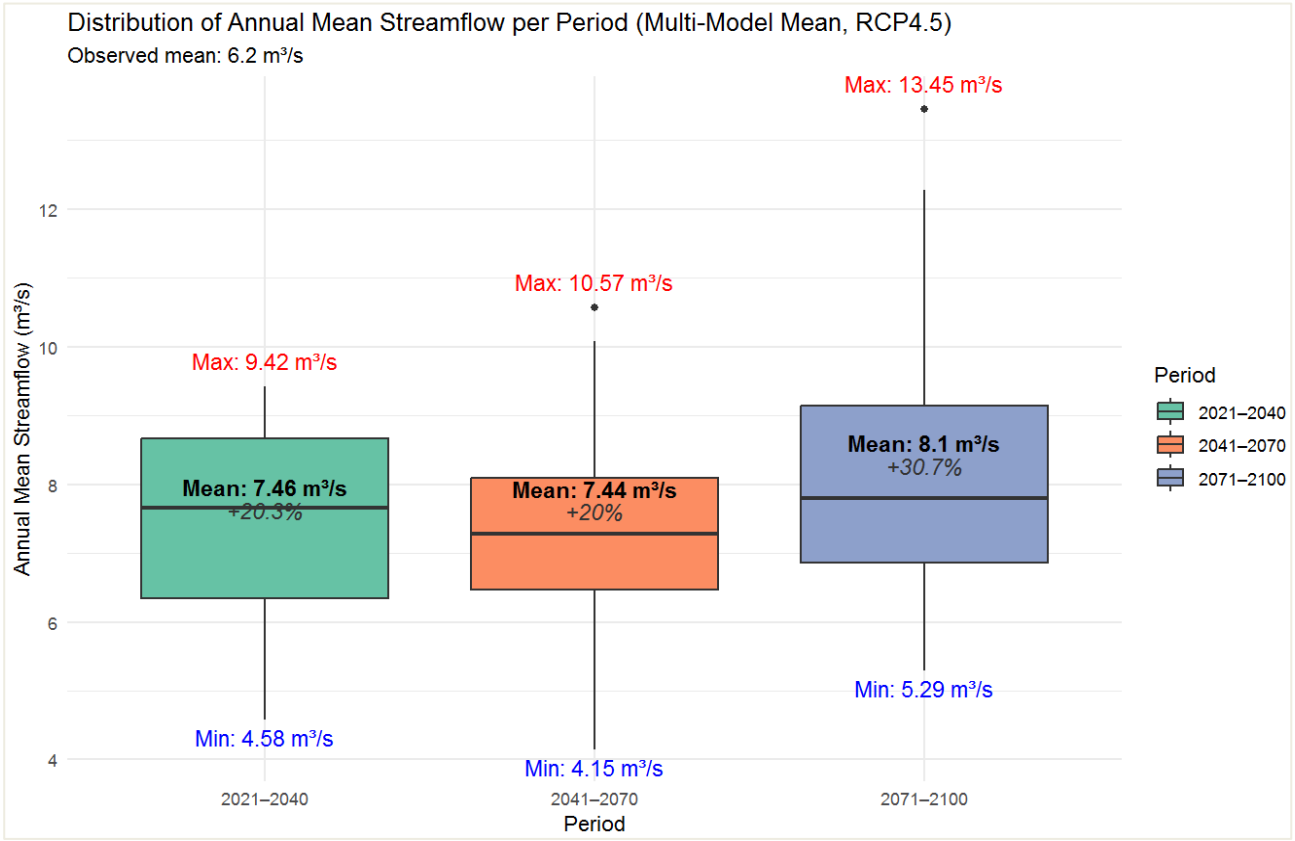

Figure 13. Projected mean annual streamflow distribution for the near-term (2021-2040), mid-century (2041-2070), and late-century (2071-2100) periods under the RCP4.5 scenario.

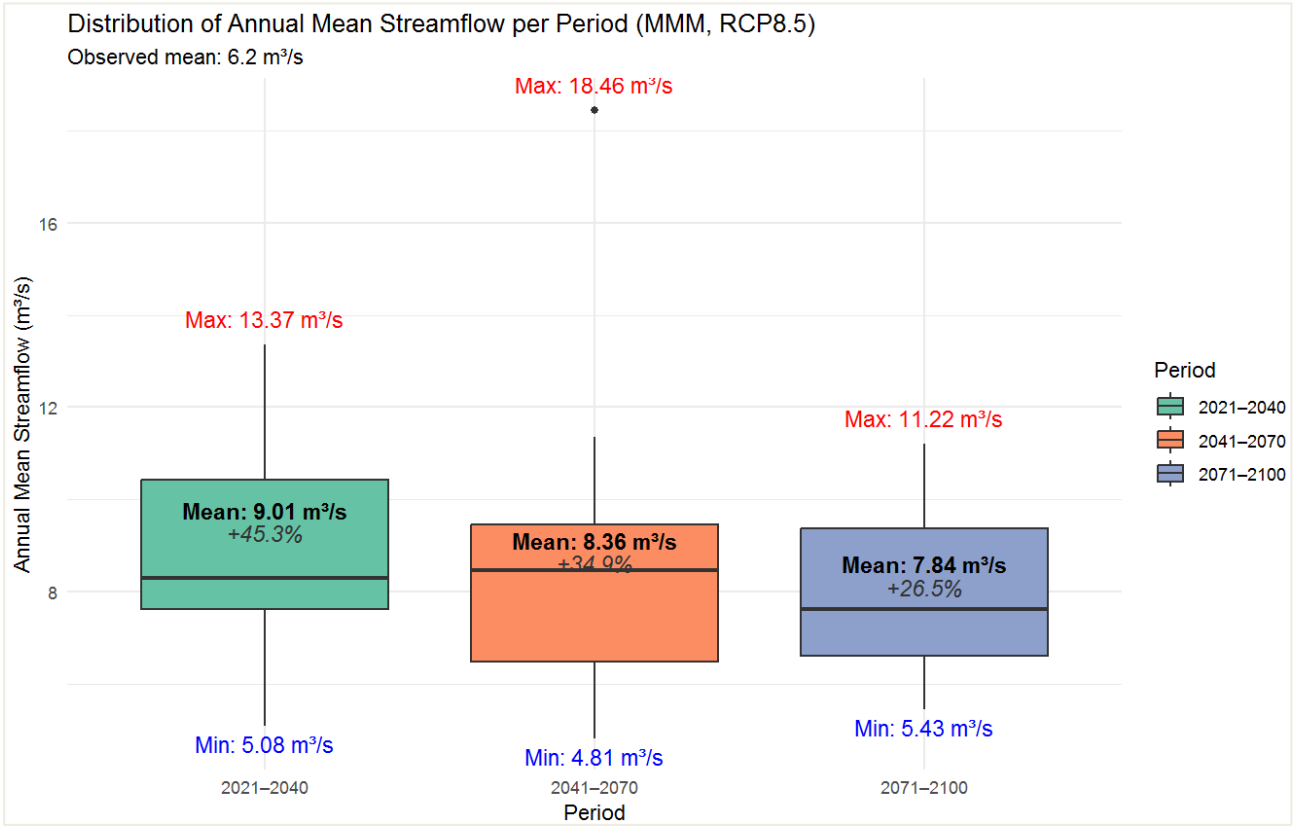

Figure 14. Projected mean annual streamflow distribution for the near term (2021-2040), mid-century (2041-2070), and late century (2071-2100) periods under the RCP8.5 scenario.

4.2.7. Hydrological Regime Variability under Future Climate Scenarios

The simulated monthly hydrographs of the Diaguiri River Basin, generated using the GR4J rainfall-runoff model driven by bias-corrected outputs from five CMIP5 climate models under RCP4.5 and RCP8.5 scenarios, indicate substantial shifts in the seasonal hydrological regime throughout the 21st century (Tables5&6). Both climate scenarios suggest a notable advancement in the onset of runoff, intensification of seasonal peak flows, and greater intra-annual variability. During the dry season (November-April), projected discharges remain low (below 1 m^3/s), yet are slightly elevated compared to the historical baseline. For instance, January flows rise from 0.13 m^3/s (observed) to 0.63 m^3/s (projected), signaling possible changes in baseflow contributions or early-season precipitation inputs. Despite low mean flows, this period exhibits pronounced interannual variability, as shown by high skewness and kurtosis—particularly in May and June, where kurtosis exceeds 21 under RCP8.5, reflecting the likelihood of rare but intense rainfall-runoff events. The onset of significant runoff is projected to shift earlier in the hydrological year. In May, average flows reach 0.38 m^3/s (RCP8.5) and 0.30 - 0.37 m^3/s (RCP4.5), up from 0.27 m^3/s observed, despite the flow regime being dominated by irregular and extreme events (CV > 2.0). This temporal advancement may reflect earlier rainfall onset and reduced soil moisture deficits, potentially altering catchment response thresholds.

Streamflow magnitudes during the peak season (July-September) show the most

dramatic changes. Under RCP8.5, mean discharges in August and September rise to 25.86 m^3/s and 35.05 m^3/s respectively, corresponding to +54.8% and +13% increases over historical levels. RCP4.5 follows similar trends, albeit with more moderate increases. These changes are accompanied by heightened standard deviation and expanded interquartile ranges, indicating stronger interannual fluctuations. While coefficients of variation remain under 1—consistent with seasonal regimes—the rise in skewness (e.g., July: 1.06) and kurtosis (e.g., October: 3.51) reveals a higher frequency of extreme high-flow events, underscoring intensifying flood risks under future climate conditions. The recession period (October-December) also presents elevated flow levels. In October, for example, RCP8.5 projections indicate mean flows of 13.53 m^3/s, compared to 11.57 m^3/s historically (+16.9%). Statistical descriptors such as skewness and kurtosis remain high in these months, highlighting the persistence of asymmetric, heavy-tailed distributions and the continued risk of late-season hydrological extremes. Figure 15 and Figure 16, which present monthly boxplots comparing historical and projected multi-model streamflow quantiles under RCP4.5 and RCP8.5, visually confirm the overall intensification of the seasonal hydrograph.

Overall, both emission scenarios forecast an intensification of runoff dynamics in the Diaguiri River Basin, characterized by heightened magnitudes, increased recurrence, and amplified variability of high-flow events. The RCP4.5 scenario suggests a moderately wetter hydrological regime accompanied by enhanced asymmetry and leptokurtic streamflow distributions, indicative of more frequent but moderate extremes. In contrast, RCP8.5 projects more severe hydrological extremes and greater inter-model and intra-annual variability, reflecting deeper distributional uncertainty. These projected transformations underscore a clear departure from historical hydrological stationarity and highlight the urgent need for flexible, adaptive water resource management strategies and robust flood risk governance tailored to the vulnerabilities of semi-humid tropical river systems such as the Diaguiri Basin.

Table 5. Monthly streamflow statistics (Mean, SD, CV, Skewness, Kurtosis) for the Diaguiri River Basin under RCP4.5

Month	Mean_RCP4.5 (m3/s)	SD (m3/s)	CV	Skewness	Kurtosis	Observed Discharge (m3/s)
Jan	0.631	0.041	0.065	0.359	−0.043	0.13
Feb	0.418	0.022	0.052	0.269	0.050	0.05
Mar	0.300	0.013	0.044	0.201	0.190	0.12
Apr	0.226	0.010	0.044	1.291	5.011	0.18
May	0.379	0.790	2.085	4.667	21.360	0.27
Jun	2.270	3.600	1.586	2.840	9.544	0.48
Jul	9.395	5.505	0.586	1.056	1.824	2.76
Aug	25.855	8.645	0.334	0.521	−0.090	16.71
Sep	35.053	9.261	0.264	0.360	−0.038	31.02
Oct	13.526	4.531	0.335	1.739	3.514	11.57
Nov	2.761	0.473	0.171	1.045	1.901	1.93
Dec	1.126	0.106	0.094	0.570	0.311	0.50

Table 6. Monthly streamflow statistics (Mean, SD, CV, Skewness, Kurtosis) for the Diaguiri River Basin under RCP8.5.

Month	Mean_RCP8.5 (m3/s)	SD (m3/s)	CV	Skewness	Kurtosis	Observed Discharge (m3/s)
Jan	0.631	0.041	0.065	0.359	-0.043	0.13
Feb	0.418	0.022	0.052	0.269	0.050	0.05
Mar	0.300	0.013	0.044	0.201	0.190	0.12
Apr	0.226	0.010	0.044	1.291	5.011	0.18
May	0.379	0.790	2.085	4.667	21.360	0.27
Jun	2.270	3.600	1.586	2.840	9.544	0.48
Jul	9.395	5.505	0.586	1.056	1.824	2.76
Aug	25.855	8.645	0.334	0.521	-0.090	16.71
Sep	35.053	9.261	0.264	0.360	-0.038	31.02
Oct	13.526	4.531	0.335	1.739	3.514	11.57
Nov	2.761	0.473	0.171	1.045	1.901	1.93
Dec	1.126	0.106	0.094	0.570	0.311	0.50

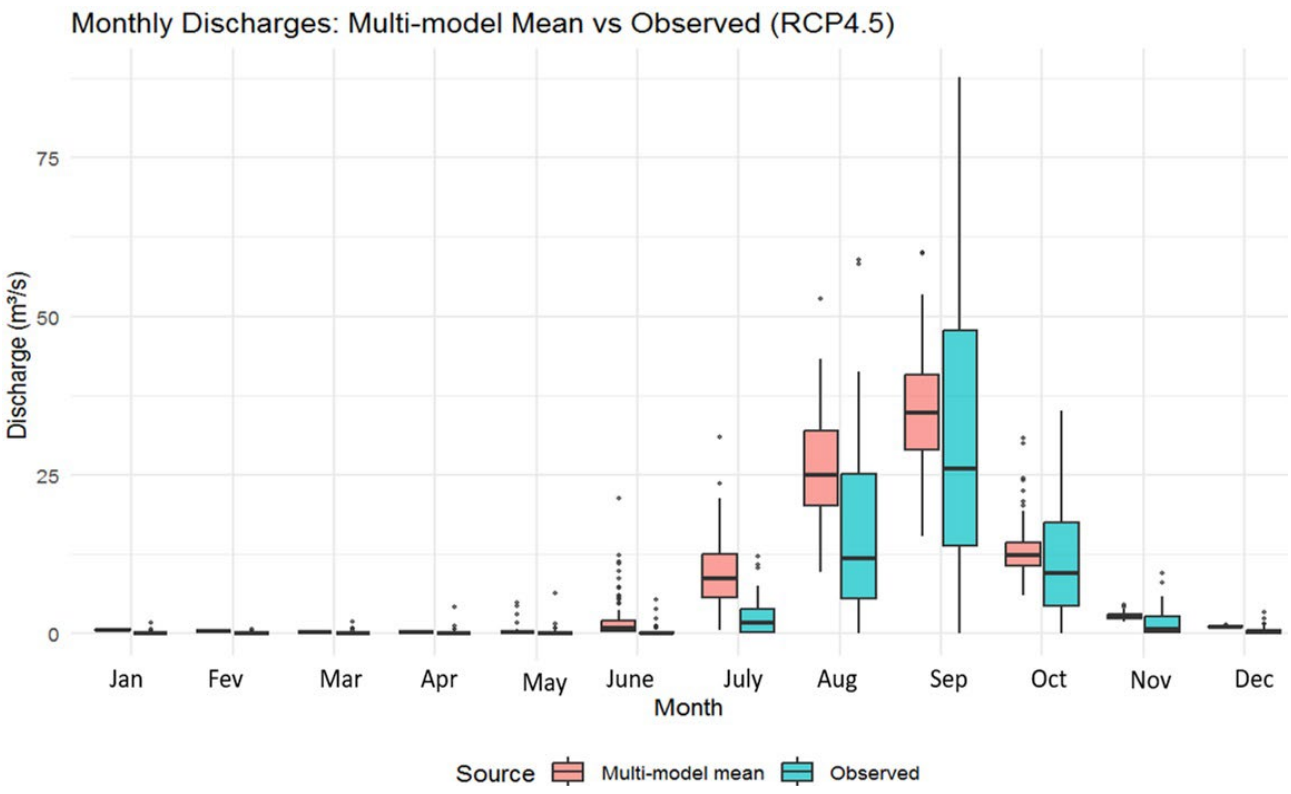

Figure 15. Boxplots comparing observed and projected monthly streamflow quantiles under the RCP4.5 scenario (multi-model mean) for the Diaguiri River Basin at the 2100 horizon.

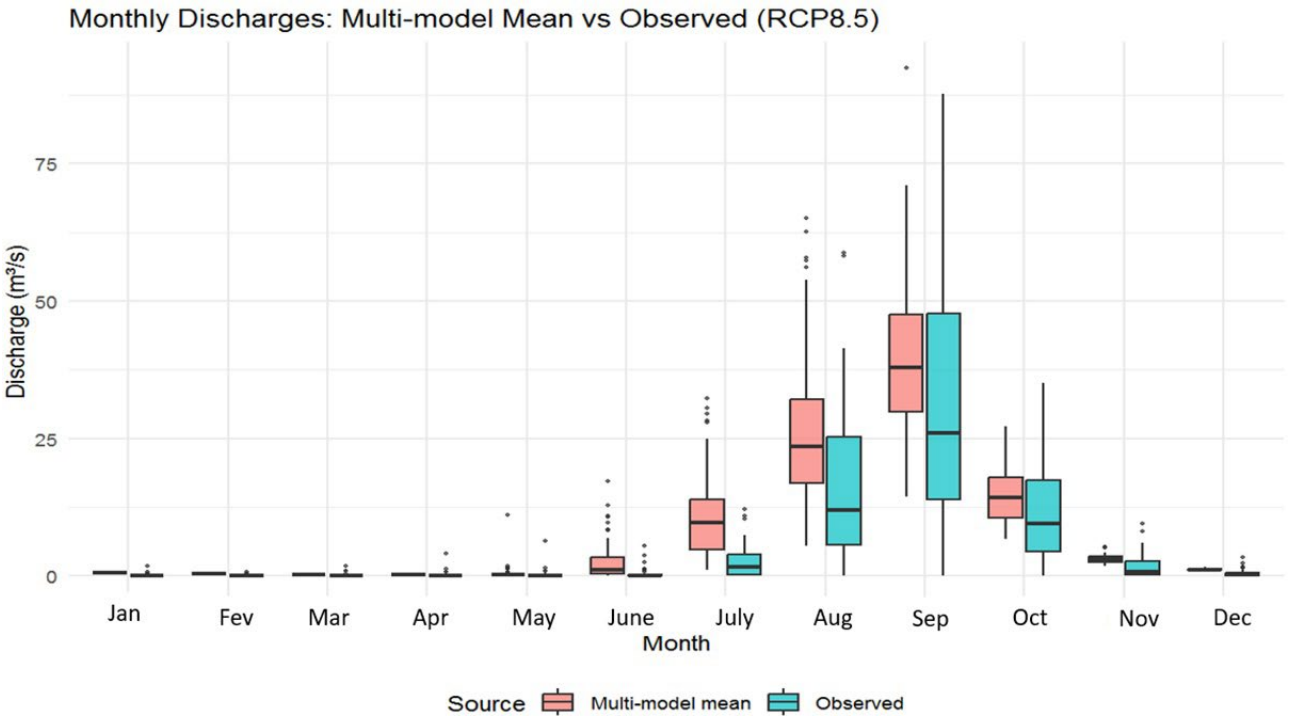

Figure 16. Boxplots comparing observed and projected monthly streamflow quantiles under the RCP8.5 scenario (multi-model mean) for the Diaguiri River Basin at the 2100 horizon.

5. Discussion

This study aimed to assess the impacts of climate change on future surface water availability in the semi-humid Diaguiri River Basin using the GR4J rainfall-runoff model driven by bias-corrected regional climate projections. The evaluation of the model's performance during the cross-validation phase offers valuable insights into its reliability and transferability across distinct climatic conditions. The cross-validation results reveal a clear improvement in model performance between the calibration (1981-1992) and validation (1998-2004) periods, indicating the GR4J model's ability to generalize across interannual hydrological variability. The increase in Nash-Sutcliffe Efficiency (NSE) from 0.66 to 0.71, along with a substantial gain in the log-NSE from 0.54 to 0.77, underscores the model's capacity to capture both peak discharge events and baseflow dynamics—an essential feature in semi-humid systems governed by the alternation between wet and dry seasons (Bodian et al., 2018; Thiaw, 2020; Thiaw et al., 2021). The Kling-Gupta Efficiency (KGE), rising from 0.71 to 0.83, and the coefficient of determination (R^2) following the same trend (0.66 to 0.71), further confirm the model's balanced performance across key hydrological components. These outcomes are in line with previous findings across West African basins and similar tropical environments (e.g., Thiaw et al., 2021; Dembélé et al., 2020; Bodian et al., 2018; Satgé et al., 2015), where GR4J has proven effective in simulating flows under data-scarce conditions. The robustness observed during validation supports the selection of the associated parameter set (X1: 207.40 mm, X2: −30.66 mm, X3: 333.28 mm, X4: 2.09 days) for

use in future climate impact simulations. This parameterization ensures methodological consistency and provides a reliable foundation for scenario-based projections. By anchoring long-term hydrological forecasts to a well-calibrated and validated model structure, this study enhances the credibility of its results and contributes to the development of adaptive water resource management strategies in the face of increasing climate uncertainty.

Following the validation of the hydrological model, bias correction was a critical step to ensure that the climate model outputs used as inputs for future hydrological simulations accurately reflected local conditions. The application of the CDF-t technique for correcting temperature and precipitation biases substantially enhanced the statistical agreement between observed and modeled climate variables, which is essential for realistic streamflow projections. Under both RCP4.5 and RCP8.5 scenarios, temperature outputs from NorESM1-M, MIROC5, and IPSL-CM5A-LR showed the best alignment with observations, as evidenced by low RMSD values (e.g., 1.38 °C for NorESM1-M) and high correlations (>0.89), reinforcing their credibility for hydrological modeling. Precipitation correction also improved variance and distribution metrics, particularly for MIROC5 and NorESM1-M, which closely matched the observed standard deviation and yielded strong correlation coefficients (0.86 and 0.83, respectively). These findings are consistent with results from West African studies such as Sylla et al. (2016), Dembélé et al. (2020) and Thiaw et al. (2021), which highlight the effectiveness of CDF-t in correcting systematic biases in CMIP5-derived precipitation and temperature across the Sahel and Sudanian zones. Compared to simpler methods like linear scaling or delta change—which have been widely used in the region (Bodian et al., 2018; Sadio et al., 2023)—CDF-t offers a more refined correction by preserving the shape of the distribution and correcting both mean and variability. However, despite its strengths, recent work by Dosio & Panitz (2016) and Nikulin et al. (2012) emphasizes the importance of multi-method assessments, as some bias correction methods may struggle with extreme events or non-stationarity. In the case of the Diaguiri Basin, the successful application of CDF-t, particularly when evaluated through Taylor diagrams, confirms its value in producing climate inputs better suited for simulating future hydrological conditions in semi-humid tropical basins. By improving the realism of future temperature and rainfall projections, bias correction directly enhances the robustness of the GR4J-based hydrological simulations, thus providing a sound basis for climate adaptation strategies and sustainable water resource planning in West Africa.

The hydrological projections for the Diaguiri River Basin under CMIP5-based RCP4.5 and RCP8.5 scenarios reveal a marked intensification of streamflow dynamics driven primarily by changes in precipitation regimes and temperature-induced evapotranspiration shifts. Under RCP4.5, the multi-model ensemble mean (MMM) indicates a substantial increase in mean annual streamflow (+24%), closely tracking the moderate precipitation rise (+8.4%) projected for the basin. This positive rainfall-runoff coupling corroborates findings from other West Af-

rican studies, which report gradual wetting trends under intermediate emission pathways (Sultan et al., 2019; Abiodun et al., 2017). Nonetheless, notable inter-model variability highlights the nonlinearity of the hydrological response: models such as MIROC5 and GFDL-ESM2M predict pronounced discharge amplifications, while others like IPSL-CM5A-LR project slight runoff reductions, echoing the complex spatial heterogeneity and climatic sensitivity characteristic of tropical basins (Taylor & Marsham, 2017; Thiaw et al., 2021). Under the high-emission RCP8.5 pathway, the hydrological signal intensifies further (+34.3% mean streamflow increase), but with greater divergence and uncertainty among models. The amplification of discharge variability suggests increased flood risk and a pronounced departure from historical hydrological stationarity. These findings align with those of Angelina et al. (2015), who reported increases in mean annual discharge of the Niger River at Koulikoro by 6.9% (2026-2050), 0.9% (2051-2075), and 5.6% (2076-2100) based on SWAT model simulations under the SRES A1B scenario. Similarly, Azari et al. (2016) projected increases in streamflow under both RCP4.5 and RCP8.5 scenarios for the Gorganroud River basin in northern Iran. Together, these studies corroborate the general trend of enhanced runoff and streamflow in response to moderate to high greenhouse gas emissions, underscoring a common pattern of hydrological intensification across diverse climatic and geographic contexts. This cross-regional consistency further supports the robustness of the GR4J model projections for the Diaguiri River Basin and reinforces the need for adaptive water resource management strategies tailored to future hydrological variability. Temporally, the streamflow response under RCP4.5 is relatively coherent and progressive across the century, whereas RCP8.5 yields a more erratic trajectory with an initial surge in runoff followed by declines linked to precipitation uncertainties. Seasonal hydrograph analyses indicate an earlier onset of runoff, elevated baseflows during the dry season, and substantially intensified peak flows in the wet season, emphasizing shifts in hydrological seasonality and extreme event frequency. These findings resonate with regional observations of changing monsoonal rainfall patterns and heightened hydrological variability in West Africa (Niang et al., 2014; Fontaine, 2012; Dia-Diop, 2020). Overall, this study highlights the critical need for integrating climate-driven hydrological uncertainty into adaptive water resource management frameworks in the Diaguiri Basin, emphasizing scenario-dependent flood risk mitigation and sustainable planning for semi-humid tropical catchments vulnerable to non-stationary climate regimes.

6. Conclusion

This study offers a detailed and robust evaluation of the impacts of climate change on the hydrological dynamics of the Diaguiri River Basin, a representative semi-humid tropical watershed in West Africa. By integrating the GR4J rainfall-runoff model with bias-corrected climate projections from a multi-model CMIP5 ensemble under both RCP4.5 and RCP8.5 scenarios, we have quantified future changes in temperature, precipitation, and streamflow characteristics through the 21st

century. The results demonstrate a clear and progressive warming trend across the basin, with temperature increases ranging from +1.3˚C to +2.4˚C under RCP4.5, and intensifying up to +4.4˚C under the high-emission RCP8.5 scenario by century's end. This warming is projected to significantly influence the basin's hydrological cycle, notably through enhanced evapotranspiration and shifts in rainfall patterns. Precipitation projections reveal more complex and uncertain trends. Under the moderate RCP4.5 pathway, a general increase in rainfall and runoff is anticipated, supporting a wetter future with an ensemble mean precipitation rise of about 8% - 12%, accompanied by a corresponding 24% increase in mean annual streamflow. This scenario suggests a relatively coherent intensification of the hydrological regime, characterized by heightened runoff volumes and moderately increased variability. In contrast, the RCP8.5 scenario presents a more heterogeneous and erratic precipitation signal, with some models projecting substantial wetting while others forecast drying trends. Consequently, streamflow projections under RCP8.5 show amplified variability and extremes, with an overall ensemble mean increase of 34%, but with significant inter-model divergence—including scenarios of both increased flooding risk and reduced water availability. Seasonal analyses further reveal shifts in the hydrological regime, with earlier onset of runoff, intensified peak flows during the rainy season, and elevated baseflows in the dry season. The projected rise in flow variability and frequency of extreme events, particularly under RCP8.5, signals a transition toward hydrological non-stationarity. This has critical implications for water resources management, flood risk mitigation, and ecosystem health in the basin. These findings underscore the necessity of incorporating climate model uncertainties and hydrological sensitivities in planning frameworks. Given the semi-humid and rainfall-dependent nature of the Diaguiri Basin, adaptive water management strategies must prioritize flexibility, enhanced monitoring, and integrated approaches that consider both climatic and socio-economic factors. Future research directions should include downscaling to finer spatial resolutions, coupling hydrological models with land use and groundwater dynamics, and engaging stakeholders to co-develop resilience pathways. Overall, this study contributes valuable insights into the evolving water cycle of a vulnerable West African basin, supporting informed decision-making to safeguard water security under uncertain but increasingly challenging climate futures.

Conflicts of Interest

The author declares no conflicts of interest regarding the publication of this paper.

References

Abiodun, B. J., Adegoke, J., Abatan, A. A., Ibe, C. A., Egbebiyi, T. S., Engelbrecht, F. et al. (2017). Potential Impacts of Climate Change on Extreme Precipitation over Four African Coastal Cities. *Climatic Change, 143,* 399-413. https://doi.org/10.1007/s10584-017-2001-5

Angelina, A., Gado Djibo, A., Seidou, O., Seidou Sanda, I., & Sittichok, K. (2015). Changes

to Flow Regime on the Niger River at Koulikoro under a Changing Climate. *Hydrological Sciences Journal, 60,* 1709-1723. https://doi.org/10.1080/02626667.2014.916407

Ayugi, B., Tan, G., Ruoyun, N., Babaousmail, H., Ojara, M., Wido, H. et al. (2020). Quantile Mapping Bias Correction on Rossby Centre Regional Climate Models for Precipitation Analysis over Kenya, East Africa. *Water, 12,* Article 801. https://doi.org/10.3390/w12030801

Azari, M., Moradi, H. R., Saghafian, B., & Faramarzi, M. (2016). Climate Change Impacts on Streamflow and Sediment Yield in the North of Iran. *Hydrological Sciences Journal, 61,* 123-133. https://doi.org/10.1080/02626667.2014.967695

Bentsen, M., Bethke, I., Debernard, J. B., Iversen, T., Kirkevåg, A., Seland, Ø. et al. (2013). The Norwegian Earth System Model, Noresm1-M—Part 1: Description and Basic Evaluation of the Physical Climate. *Geoscientific Model Development, 6,* 687-720. https://doi.org/10.5194/gmd-6-687-2013

Beven, K. (2012). *Rainfall-Runoff Modelling: The Primer* (2nd éd.). Wiley. https://doi.org/10.1002/9781119951001

Bodian, A., Dezetter, A., Diop, L., Deme, A., Djaman, K., & Diop, A. (2018). Future Climate Change Impacts on Streamflows of Two Main West Africa River Basins: Senegal and Gambia. *Hydrology, 5,* Article 21. https://doi.org/10.3390/hydrology5010021

Cannon, A. J. (2018). Multivariate Quantile Mapping Bias Correction: An N-Dimensional Probability Density Function Transform for Climate Model Simulations of Multiple Variables. *Climate Dynamics, 50,* 1735-1750.

Cannon, A. J., Sobie, S. R., & Murdock, T. Q. (2015). Bias Correction of GCM Precipitation by Quantile Mapping: How Well Do Methods Preserve Changes in Quantiles and Extremes? *Journal of Climate, 28,* 6938-6959. https://doi.org/10.1175/jcli-d-14-00754.1

Collins, W. J., Bellouin, N., Doutriaux-Boucher, M., Gedney, N., Halloran, P., Hinton, T. et al. (2011). Development and Evaluation of an Earth-System Model—Hadgem2. *Geoscientific Model Development, 4,* 1051-1075. https://doi.org/10.5194/gmd-4-1051-2011

Coron, L., Thirel, G., Delaigue, O., Perrin, C., & Andréassian, V. (2017). The Suite of Lumped GR Hydrological Models in an R Package. *Environmental Modelling & Software, 94,* 166-171. https://doi.org/10.1016/j.envsoft.2017.05.002

Dembélé, M., Schaefli, B., van de Giesen, N., & Mariéthoz, G. (2020). Suitability of 17 Gridded Rainfall and Temperature Datasets for Large-Scale Hydrological Modelling in West Africa. *Hydrology and Earth System Sciences, 24,* 5379-5406. https://doi.org/10.5194/hess-24-5379-2020

Déqué, M. (2007). Frequency of Precipitation and Temperature Extremes over France in an Anthropogenic Scenario: Model Results and Statistical Correction According to Observed Values. *Global and Planetary Change, 57,* 16-26. https://doi.org/10.1016/j.gloplacha.2006.11.030

Dia-Diop, A., Zebaze, S., Wade, M., Djiondo, R. N., Diop, B., Efon, E. et al. (2020). Interannual Variability of Rainfall over the West Africa Sahel. *Journal of Geoscience and Environment Protection, 8,* 85-101. https://doi.org/10.4236/gep.2020.83007

Diallo, I., Giorgi, F., Diba, I., Camara, M., & Torma, C. (2016). Uncertainties in the Late Twenty-First Century Climate Change Projections over Africa. *Climate Dynamics, 47,* 2935-2954.

Dosio, A. (2017). Climate Simulations at High Resolution over West Africa: Representation of the West African Monsoon and Regional Precipitation Patterns. *Climate Dynamics, 48,* 2287-2308.

Dosio, A., & Panitz, H. (2015). Climate Change Projections for Cordex-Africa with

COSMO-CLM Regional Climate Model and Differences with the Driving Global Climate Models. *Climate Dynamics, 46,* 1599-1625. https://doi.org/10.1007/s00382-015-2664-4

Dosio, A., Jones, R. G., Jack, C., Lennard, C., Nikulin, G., & Hewitson, B. (2015). What Can We Know about Future Precipitation in Africa? Robustness, Significance and Added Value of Projections from a Large Ensemble of Regional Climate Models. *Climate Dynamics, 49,* 711-726.

Duan, Q., Sorooshian, S., & Gupta, V. K. (1994). Optimal Use of the SCE-UA Global Optimization Method for Calibrating Watershed Models. *Journal of Hydrology, 158,* 265-284. https://doi.org/10.1016/0022-1694(94)90057-4

Dufresne, J., Foujols, M., Denvil, S., Caubel, A., Marti, O., Aumont, O. et al. (2013). Climate Change Projections Using the IPSL-CM5 Earth System Model: From CMIP3 to Cmip5. *Climate Dynamics, 40,* 2123-2165. https://doi.org/10.1007/s00382-012-1636-1

Dunne, J. P., John, J. G., Adcroft, A. J., Griffies, S. M., Hallberg, R. W., Shevliakova, E. et al. (2012). GFDL's ESM2 Global Coupled Climate-Carbon Earth System Models. Part I: Physical Formulation and Baseline Simulation Characteristics. *Journal of Climate, 25,* 6646-6665. https://doi.org/10.1175/jcli-d-11-00560.1

Ehret, U., Zehe, E., Wulfmeyer, V., Warrach-Sagi, K., & Liebert, J. (2012). HESS Opinions "Should We Apply Bias Correction to Global and Regional Climate Model Data?". *Hydrology and Earth System Sciences, 16,* 3391-3404. https://doi.org/10.5194/hess-16-3391-2012

Faye, C., & Mendy, A. (2018). Climatic Variability and Hydrological Impacts in West Africa: Case of the Gambia Watershed (Senegal). *Environmental and Water Sciences, public Health and Territorial Intelligence Journal, 2,* 54-66.

Fontaine, B., Roucou, P., Camara, M., Vigaud, N., Konaré, A., Sanda, S. I. et al. (2012). Variabilité pluviométrique, changement climatique et régionalisation en région de mousson africaine. *La Météorologie, 8,* 41. https://doi.org/10.4267/2042/48131

Giorgi, F., & Mearns, L. O. (1999). Introduction to Special Section: Regional Climate Modeling Revisited. *Journal of Geophysical Research: Atmospheres, 104,* 6335-6352. https://doi.org/10.1029/98jd02072

Giorgi, F., Jones, C., & Asrar, G. R. (2009). Addressing Climate Information Needs at the Regional Level: The CORDEX Framework. *World Meteorological Organization Bulletin, 58,* 175-183.

Gogien, F. (2023). *Impact des séries chronologiques de pluies futures à horizon 2100 sur les déversements des réseaux d'assainissement.* INSA de Lyon.

Gogien, F., Dechesne, M., Martinerie, R., & Lipeme Kouyi, G. (2023). Assessing the Impact of Climate Change on Combined Sewer Overflows Based on Small Time Step Future Rainfall Timeseries and Long-Term Continuous Sewer Network Modelling. *Water Research, 230,* 119504. https://doi.org/10.1016/j.watres.2022.119504

Gudmundsson, L., Bremnes, J. B., Haugen, J. E., & Engen-Skaugen, T. (2012). Technical Note: Downscaling RCM Precipitation to the Station Scale Using Statistical Transformations—A Comparison of Methods. *Hydrology and Earth System Sciences, 16,* 3383-3390. https://doi.org/10.5194/hess-16-3383-2012

Gupta, H. V., Kling, H., Yilmaz, K. K., & Martinez, G. F. (2009). Decomposition of the Mean Squared Error and NSE Performance Criteria: Implications for Improving Hydrological Modelling. *Journal of Hydrology, 377,* 80-91. https://doi.org/10.1016/j.jhydrol.2009.08.003

Kling, H., Fuchs, M., & Paulin, M. (2012). Runoff Conditions in the Upper Danube Basin under an Ensemble of Climate Change Scenarios. *Journal of Hydrology, 424,* 264-277.

https://doi.org/10.1016/j.jhydrol.2012.01.011

Kotlarski, S., Keuler, K., Christensen, O. B., Colette, A., Déqué, M., Gobiet, A. et al. (2014). Regional Climate Modeling on European Scales: A Joint Standard Evaluation of the EURO-CORDEX RCM Ensemble. *Geoscientific Model Development, 7,* 1297-1333. https://doi.org/10.5194/gmd-7-1297-2014

Legates, D. R., & McCabe, G. J. (1999). Evaluating the Use of "Goodness-Of-Fit" Measures in Hydrologic and Hydroclimatic Model Validation. *Water Resources Research, 35,* 233-241. https://doi.org/10.1029/1998wr900018

Maraun, D., Wetterhall, F., Ireson, A. M., Chandler, R. E., Kendon, E. J., Widmann, M. et al. (2010). Precipitation Downscaling under Climate Change: Recent Developments to Bridge the Gap between Dynamical Models and the End User. *Reviews of Geophysics, 48,* RG3003. https://doi.org/10.1029/2009rg000314

Michelangeli, P., Vrac, M., & Loukos, H. (2009). Probabilistic Downscaling Approaches: Application to Wind Cumulative Distribution Functions. *Geophysical Research Letters, 36,* L11708. https://doi.org/10.1029/2009gl038401

Moriasi, D. N., Arnold, J. G., Van Liew, M. W., Bingner, R. L., Harmel, R. D., & Veith, T. L. (2007). Model Evaluation Guidelines for Systematic Quantification of Accuracy in Watershed Simulations. *Transactions of the ASABE, 50,* 885-900. https://doi.org/10.13031/2013.23153

Nash, J. E., & Sutcliffe, J. V. (1970). River Flow Forecasting through Conceptual Models Part I—A Discussion of Principles. *Journal of Hydrology, 10,* 282-290. https://doi.org/10.1016/0022-1694(70)90255-6

Niang, I., Ruppel, O. C., Abdrabo, M. A., Essel, A., Lennard, C., Padgham, J., & Urquhart, P. (2014). Impacts, Adaptation and Vulnerability. In *Climate Change 2014: Impacts, Adaptation, and Vulnerability. Part B: Regional Aspects. Contribution of Working Group II to the Fifth Assessment Report of the Intergovernmental Panel on Climate Change* (pp. 1199-1265). Cambridge University Press.

Nikulin, G., Jones, C., Giorgi, F., Asrar, G., Büchner, M., Cerezo-Mota, R. et al. (2012). Precipitation Climatology in an Ensemble of Cordex-Africa Regional Climate Simulations. *Journal of Climate, 25,* 6057-6078. https://doi.org/10.1175/jcli-d-11-00375.1

Nka, B. N., Oudin, L., Karambiri, H., Paturel, J. E., & Ribstein, P. (2015). Trends in Floods in West Africa: Analysis Based on 11 Catchments in the Region. *Hydrology and Earth System Sciences, 19,* 4707-4719. https://doi.org/10.5194/hess-19-4707-2015

Oudin, L. (2005). *Recherche d'un modèle d'évapotranspiration potentielle pertinent comme entrée d'un modèle pluie-débit global.* Master's Thesis, Ecole Nationale du Génie Rural, des Eaux et Forêts.

Perrin, C., Michel, C., & Andréassian, V. (2003). Improvement of a Parsimonious Model for Streamflow Simulation. *Journal of Hydrology, 279,* 275-289. https://doi.org/10.1016/s0022-1694(03)00225-7

Piani, C., Weedon, G. P., Best, M. J., Gomes, S. M., Viterbo, P., Hagemann, S., & Haerter, J. O. (2010). Statistical Bias Correction of Global Simulated Daily Precipitation and Temperature for the Application of Hydrological Climate Change Impact Studies. *Journal of Hydrology, 395,* 199-215.

Pushpalatha, R., Solomatine, D. P., & Price, R. K. (2012). Improving the Calibration Efficiency of Complex Hydrological Models Using Surrogate Models. *Environmental Modelling & Software, 37,* 287-296.

Quesada-Chacón, D., Martínez Beltrán, F. J., & Gómez, M. (2021). Assessment of the Im-

pact of Climate Change on Current and Future Hydrological Regimes Using GCMs and RCMs. *Journal of Water and Climate Change, 12,* 789-806.

Refsgaard, J. C., & Knudsen, J. (1996). Operational Validation and Intercomparison of Different Types of Hydrological Models. *Water Resources Research, 32,* 2189-2202. https://doi.org/10.1029/96wr00896

Sadio, C. A. A. S., Faye, C., Pande, C. B., Tolche, A. D., Ali, M. S., Cabral-Pinto, M. M. S. et al. (2023). Hydrological Response of Tropical Rivers Basins to Climate Change Using the GR2M Model: The Case of the Casamance and Kayanga-Géva Rivers Basins. *Environmental Sciences Europe, 35,* Article No. 113. https://doi.org/10.1186/s12302-023-00822-4

Satgé, Y., Michotey, R., & Vieux, B. (2015). Application of GR4J in Tropical Basins: Evaluation in the Caraïbes Region. *Hydrological Processes, 29,* 2461-2472.

Sultan, B., Defrance, D., & Iizumi, T. (2019). Evidence of Crop-Climate Relationships in West Africa under RCP4.5 and RCP8.5 Scenarios. *Journal of Climate, 32,* 7813-7831.

Sy, K. (2019) :Effets du réchauffement global de 1.5 et 2.0°C sur l'hydrologie du bassin versant de la Falémé; Mémoire de Master 2, Université Assane Seck de Ziguinchor, Sénégal, 54p (In French)

Sylla, M. B., Dosio, A., & Diedhiou, A. (2015). Climate Change Projections over West Africa: Emerging Trends from CORDEX Regional Climate Models. *Climate Research, 64,* 143-162.

Sylla, M. B., Giorgi, F., Pal, J. S., & Gibba, P. (2013). Projected Changes in the Annual Cycle of High-Intensity Precipitation Events over West Africa for the Late Twenty-First Century. *Journal of Climate, 26,* 9597-9611.

Sylla, M. B., Nikiema, P. M., Gibba, P., Kebe, I., & Klutse, N. A. B. (2016). Climate Change over West Africa: Recent Trends and Future Projections. In J. A. Yaro, & J. Hes-selberg (Eds.), *Adaptation to Climate Change and Variability in Rural West Africa* (pp. 25-40). Springer International Publishing. https://doi.org/10.1007/978-3-319-31499-0_3

Taylor, C. M., & Marsham, J. H. (2017). Frequency of Extreme Sahelian Storms Tripled Since 1982 in Satellite Observations. *Geophysical Research Letters, 44,* 8510-8517.

Teutschbein, C., & Seibert, J. (2012). Bias Correction of Regional Climate Model Simulations for Hydrological Climate-Change Impact Studies: Review and Evaluation of Different Methods. *Journal of Hydrology, 456,* 12-29. https://doi.org/10.1016/j.jhydrol.2012.05.052

Thiaw, I. (2020). *Caractérisation et Valorisation des Ressources en Eau des Bas-Fonds du Bassin Versant du Diarha.* Master's Thesis, Université Cheikh Anta Diop de Dakar.

Thiaw, I., Faty, B., Dacosta, H., Mendy, A., Manga, A. V., & Sow, A. A. (2021). Assessment of Hydrological Impacts of Climate Change on the Diarha Watershed. In S. Diop, P. Scheren, & A. Niang (Eds.), *Climate Change and Water Resources in Africa* (pp. 277-308). Springer International Publishing. https://doi.org/10.1007/978-3-030-61225-2_13

Vauchel, P. (2004). *Hydraccess: Logiciel d'importation, de stockage et de traitement de bases de données.* IRD.

Vrac, M., & Friederichs, P. (2015). Multivariate Bias Correction of Climate Simulations: Coupling Haar Wavelets and Empirical Copulas. *Hydrology and Earth System Sciences, 19,* 1-17.

Vrac, M., Drobinski, P., Merlo, A., Herrmann, M., Lavaysse, C., Li, L. et al. (2012). Dynamical and Statistical Downscaling of the French Mediterranean Climate: Uncertainty Assessment. *Natural Hazards and Earth System Sciences, 12,* 2769-2784. https://doi.org/10.5194/nhess-12-2769-2012

Vrugt, J. A., Gupta, H. V., Bouten, W., & Sorooshian, S. (2003). A Shuffled Complex Evolution Metropolis Algorithm for Optimization and Uncertainty Assessment of Hydrologic Model Parameters. *Water Resources Research, 39,* Article No. 1201. https://doi.org/10.1029/2002wr001642

Watanabe, M., Suzuki, T., O'ishi, R., Komuro, Y., Watanabe, S., Emori, S. et al. (2010). Improved Climate Simulation by MIROC5: Mean States, Variability, and Climate Sensitivity. *Journal of Climate, 23,* 6312-6335. https://doi.org/10.1175/2010jcli3679.1

Wilby, R. L., Dawson, C. W., & Barrow, E. M. (2004). SDSM—A Decision Support Tool for the Assessment of Regional Climate Change Impacts. *Environmental Modelling & Software, 17,* 145-157. https://doi.org/10.1016/s1364-8152(01)00060-3

Zubler, E. M., Schär, C., & Lüthi, D. (2016). Resolution Limitations of Global Climate Models for Hydrological Impact Studies: GCMs Operate at Coarse Horizontal Scales (~100-300 km), Which Constrain Their Usefulness at Watershed or Local Scales. *Environmental Research Letters, 11,* Article ID: 084015.